JOURNAL OF GUIDANCE, CONTROL, AND DYNAMICS
Vol. 27, No. 3, May–June 2004

Dual-Controller Approach to Three-Dimensional Autonomous Formation Control

Erfu Yang
Tokyo Institute of Technology, Tokyo 152-0033, Japan
Yoichiro Masuko
Mitsubishi Heavy Industries, Ltd., Nagoya 455-8515, Japan
and
Tsutomu Mita
Tokyo Institute of Technology, Tokyo 152-0033, Japan

The formation-keeping control problem is addressed for the three-dimensional autonomous formation flight of multiple aircraft. The full nonlinear kinematics model describing the relative position and orientation of the formation flight system is used to develop the nonlinear formation-keeping controllers. To deal with the input–output invertibility problem of the formation control system under consideration, a dual-controller approach is presented in this study. First, the original nonlinear formation system is decomposed into two subsystems. Next, the corresponding controller for each subsystem is developed. By invoking the nonlinear dynamic inversion-based control scheme and the well-known structure algorithm, an output-tracking controller with asymptotic stability is achieved for the first subsystem. The second subsystem is simple, and a relative roll angle-hold controller is designed to achieve an exponential convergence rate. Simulation results are provided to demonstrate the effectiveness of the proposed approach.

Erfu Yang was born in Gansu Province, People's Republic of China, in 1970. He received the B.E., M.E., and Ph.D. degrees from the School of Space Technology, Beijing University of Aeronautics and Astronautics, Beijing, People's Republic of China, in 1994, 1996, and 1999, respectively. From September 1999 to October 2001, he was a Postdoctoral Researcher at the Department of Automation, Tsinghua University, Beijing, People's Republic of China. As a JSPS (Japan Society for the Promotion of Science) Postdoctoral Research Fellow, from November 2001 to December 2003 he worked in the Department of Mechanical and Control Systems Engineering at the Tokyo Institute of Technology, Tokyo, Japan. His research interests include nonlinear control theory and applications, process modeling and control, fault diagnosis, and safety monitoring. He is a member of AIAA and the Society of Instrument and Control Engineers. E-mail: yef@ctrl.titech.ac.jp.

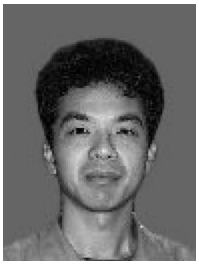

Yoichiro Masuko received his B.A. in electronic engineering from Chiba University, Chiba, Japan, in 1991. Since 1991, he has been designing flight control systems at Mitsubishi Heavy Industries, Ltd., Nagoya, Japan. His research interests include robust control and nonlinear control theory. He is a member of the Japan Society for Aeronautical and Space Sciences. E-mail: yoichiro_masuko@mx.nasw.mhi.co.jp.

Tsutomu Mita received the Dr. Eng. degree in electrical engineering from the Tokyo Institute of Technology, Tokyo, Japan, in 1975. From 1975 to 1995, he was with the Chiba University, Chiba, Japan. Since 1995, he has been a Professor in the Department of Mechanical and Control Systems Engineering, Tokyo Institute of Technology. His current research interests are in nonlinear control theory and robotics. He is a member of the Institute of Electrical and Electronics Engineers, the Society of Instrument and Control Engineers, the Institute of Electrical Engineers of Japan, and the Robotics Society of Japan. E-mail: mita@ctrl.titech.ac.jp.

Received 31 March 2003; revision received 25 June 2003; accepted for publication 25 June 2003; presented as Paper 2003-PP7453 at the AIAA/ICAS International Air and Space Symposium and Exposition: The Next 100 Years, Dayton, Ohio, 14–17 July 2003. Copyright © 2003 by the authors. Published by the American Institute of Aeronautics and Astronautics, Inc., with permission. Copies of this paper may be made for personal or internal use, on condition that the copier pay the $10.00 per-copy fee to the Copyright Clearance Center, Inc., 222 Rosewood Drive, Danvers, MA 01923; include the code 0731-5090/04 $10.00 in correspondence with the CCC.

Nomenclature

$\boldsymbol{C}_\alpha, \boldsymbol{D}_\alpha, \boldsymbol{H}_\alpha$	=	matrices resulted from the structure algorithm
$D_\alpha^\dagger$	=	left or right inverse
d_i	=	distance between actual and desired position, m
$\boldsymbol{f}, \boldsymbol{g}, \boldsymbol{h}$	=	representation of the original system or a generic nonlinear affine system
$\tilde{\boldsymbol{f}}, \tilde{\boldsymbol{g}}, \tilde{\boldsymbol{h}}$	=	representation of the subsystem $\boldsymbol{I}$
$\mathbb{G}$	=	Lie group
g	=	configuration of one rigid body in Lie group
K	=	design parameter of ϕ_{ri}-hold controller
$L_f^k \boldsymbol{g}(x)$	=	kth Lie derivative of $\boldsymbol{g}(\boldsymbol{x})$ along a vector field $\boldsymbol{f}(\boldsymbol{x})$
$\mathbb{M}, \tilde{\mathbb{M}}, \mathbb{Y}$	=	manifolds
$N+1$	=	aircraft number of the fleet
n_j, N_j	=	lowest- and highest-order derivative of output y_j, respectively
$\boldsymbol{q}_i$	=	vector of relative position with respect to referential aircraft
R_i	=	collision safety radius of aircraft i with respect to its desired position, m
T_1, T_2, T_3	=	time constants, s
t	=	time, s
$\boldsymbol{u}, \tilde{\boldsymbol{u}}$	=	vectors of control input
v_0, v_i	=	translational velocities of referential aircraft 0 and aircraft i, m/s
$\bar{v}_i$	=	translational velocity limit of aircraft i, m/s
$w_{j,k}$	=	design parameters of perturbation controller
$\boldsymbol{x}, \tilde{\boldsymbol{x}}$	=	state vectors
$x_{\text{ri}}, y_{\text{ri}}, z_{\text{ri}}$	=	relative position of aircraft i with respect to referential aircraft 0, m
$\boldsymbol{y}, \tilde{\boldsymbol{y}}$	=	vectors of output
$\beta_{j,k}$	=	coefficients of Hurwitz polynomials
$\boldsymbol{\rho}(\boldsymbol{x})$	=	decoupling matrix
$\boldsymbol{\sigma}$	=	vector relative degree
$\phi_{\text{ri}}, \psi_{\text{ri}}, \theta_{\text{ri}}$	=	relative orientation of aircraft i with respect to referential aircraft 0, rad
χ	=	Lie algebra
$\omega_1^i, \omega_2^i, \omega_3^i$	=	rotational velocities of aircraft i, rad/s
$\bar{\omega}_1^i, \bar{\omega}_2^i, \bar{\omega}_3^i$	=	rotational velocity bounds of aircraft i, rad/s
$\omega_1^0, \omega_2^0, \omega_3^0$	=	rotational velocities of referential aircraft 0, rad/s

Subscripts

E	=	Earth
i	=	aircraft i
L	=	leader
p	=	perturbation
R	=	reference input
r	=	relative
W	=	wingman
W_i	=	wind of the ith aircraft
α	=	relative order
0	=	referential aircraft

Superscripts

d	=	desired
T	=	transpose operator
σ_j	=	relative degree

I. Introduction

THE autonomous formation flight (AFF) of multiple aircraft has received considerable attention during the last decade.[1–5] An important reason for wider interest in the AFF is that the follower aircraft in an appropriate fleet can achieve a significant reduction in power demand. By applying the close AFF techniques to the tests, NASA's Dryden Flight Research Center has demonstrated that the trailing aircraft could save up to 15% fuel during cruise flight (data available online at http://www.aerospace.nasa.gov and at http://www.dfrc.nasa.gov). Close AFF technology also can be applied to commercial transport aircraft for typical transcontinental routes. If so, the air traffic system capacity could be substantially increased. It is estimated that close AFF can save $0.5 million on fuel costs and reduce the emission of carbon dioxide and the emission of nitrous oxide compound by 10 million lb and 0.1 million lb per trailing aircraft per year, respectively (data available online at http://www.aerospace.nasa.gov and at http://www.dfrc.nasa.gov).

Although the AFF has many benefits arising from the aforementioned aspects, there are still a number of challenges to its successful applications. Among them, formation-keeping control is a crucial challenge. Formation-keeping control can be described as how to keep the relative position and/or attitude of one aircraft (target aircraft) to another aircraft (referential aircraft). "Leader–follower" is a well-known type of formation flight by designating the referential aircraft as the leader and the target aircraft as the follower. For such a typical formation flight the performance of formation flight is tightly related with formation-keeping control. In Refs. 3 and 6, for instance, it was reported that there exists an optimal separation geometry which must be maintained to tight tolerances to achieve the maximal drag reduction from flying-in-close formation: the follower is to be placed in the same $x-y$ plane as the leader with a longitudinal separation distance of three times leader's wing span and a lateral separation distance of approximately $\pi/4$ times leader's wing span. Besides close formation flight, formation-keeping control is also crucial in developing air-to-air refueling technology. Moreover, air force fighters can use formation-keeping control to enhance its searching ability that is affected by its position in the fleet.[7]

The most current solutions toward formation-keeping control are based on linear system theory.[1–5] The traditional methods, such as proportional-integral algorithm and linear quadratic regulator, are usually adopted by many researchers to deal with nonlinearities in the formation dynamics.[1,2] For example, some linearized dynamics were assumed as follows[1,3,4]:

$$\begin{aligned}
\dot{\psi}_W &= -\left(1/\tau_{\psi_W}\right)\psi_W + \left(1/\tau_{\psi_W}\right)\psi_{W_c} \\
\dot{V}_W &= -\left(1/\tau_{V_W}\right)V_W + \left(1/\tau_{V_W}\right)V_{W_c} \\
\dot{\psi}_L &= -\left(1/\tau_{\psi_L}\right)\psi_L + \left(1/\tau_{\psi_L}\right)\psi_{L_c} \\
\dot{V}_L &= -\left(1/\tau_{V_L}\right)V_L + \left(1/\tau_{V_L}\right)V_{L_c}
\end{aligned} \tag{1}$$

where ψ_{W_c}, V_{W_c}, ψ_{L_c}, V_{L_c} are command inputs and ψ_W, V_W, ψ_L, V_L are related states for leader and wingman, respectively. One can find that it is difficult to determine the response time constants τ_{ψ_W}, τ_{V_W}, τ_{ψ_L}, τ_{V_L} precisely, which might depend on specific aircraft and flight condition as well as the performance of aircraft autopilot system.

Because linear models cannot precisely reflect the nonlinearities of autonomous formation flight, currently nonlinear control theory has attracted a great deal of attention. Based on nonlinear control theory, several approaches toward formation-keeping control have been presented (for example, see Refs. 8–10). In Ref. 8, the nonlinear control problem of multiple unmanned aerial vehicles (UAVs) in close-coupled formation flight was studied. The work in Ref. 9 presented the research on decentralized adaptive close formation control of UAVs. The input–output invertibility and sliding mode control for close formation flying of multiple UAVs were addressed in Ref. 10. Without doubt, these studies have really made a go of applying nonlinear control theory to the AFF. However, nonlinear control theory has not been exploited to its full potential in the problem of multiple aircraft formation flight. Reviewing the current state, it appears that many issues in the area of nonlinear formation flight still remain open, such as nonlinear formation keeping, output tracking, collision avoidance, and so on.

In this study we will not use any assumed formation dynamics as in Eq. (1). To develop a nonlinear formation-keeping control law, the full nonlinear kinematics model describing the relative position and orientation of the formation flight system is utilized. In comparison to the works in Refs. 1, 3, and 4, the velocities of follower aircraft are directly treated as the control inputs, which can serve as the command inputs to the basic aircraft flight-control system (AFCS), that

is, aircraft inner-loop autopilot system. Thus, in the formation flight level it is possible to derive a class of generic nonlinear control laws that only depend on the relative kinematics. From such a point of view, the controllers obtained for the three-dimensional autonomous formation flight will be only kinematics dependent, which means that no real aircraft aeronautical dynamics is needed during the design of formation-keeping control laws. The advantage is that we do not require any detailed information on the specific aircraft in the fleet, such as structure sizes, aerodynamics, propulsive power, flight conditions, and so on. In other words, it is general enough to be applied to different aircraft and would be helpful to develop a plug-and-play module for the formation flight applications.

For this purpose we introduce a new approach to the three-dimensional autonomous formation control problem in this paper. This approach is composed of two controllers: one serves as a relative roll angle-hold autopilot (hereafter it is referred to $\phi_{\mathrm{ri}}-$ hold controller), and another is an output-tracking controller, which zeros the errors between the actual and desired relative positions with respect to the referential aircraft. To design the output-tracking controller, the nonlinear dynamic inversion (NDI) technique and the well-known structure algorithm are used. The $\phi_{\mathrm{ri}}-$ hold controller is achieved by taking advantage of partial state feedback and input feedforward of the output-tracking controller. During the development of our control scheme, we assume that all of the required control inputs for formation flight can be supplied by the lower control system, namely, AFCS. Moreover, we consider that there are no collisions among the participating aircraft in the fleet.

Nonlinear dynamic inversion as a practical and viable method has been employed to many nonlinear control applications by many scholars.[11–13] However, to our knowledge the existing works in aerospace engineering are commonly focused on the traditional flight control problems rather than the formation flight control issues. In addition, most inversion-based methods usually require that the concerned nonlinear system has a well-defined vector relative degree and a nonsingular decoupling matrix.[13]

In this study the main difficulties for the system under consideration exist in the following two aspects. One is that the original system has a singular decoupling matrix and does not have a well-defined vector relative degree. Thus, the standard output-tracking methods based on nonlinear dynamic inversion scheme will break down. Another difficulty arises from the fact that the direct use of the well-known structure algorithm, a popular method for solving the singularity of decoupling matrix, also fails to obtain a nonlinear dynamic inversion for the original system. The main contribution of this paper lies in presenting a new approach to the three-dimensional autonomous formation control by solving the aforementioned difficulties.

This article is organized as follows. The full relative kinematics model from Refs. 14–16 is given in Sec. II. In Sec. III the control problem is formulated, and the existing difficulties are pointed out in detail. The dual-controller approach and control tasks' decomposition are developed in Sec. IV. The design and analysis of output-tracking controller with NDI are presented in Sec. V. In Sec. VI we deal with the design and analysis of $\phi_{\mathrm{ri}}-$ hold controller. In Sec. VII simulation results are provided to illustrate the performance of the proposed approach. Some conclusions and suggestions for further research are contained in Sec. VIII. For the reader's convenience a brief introduction to the structure algorithm is given in Appendix A.

II. Mathematical Model

Let us consider an autonomous formation of $(N+1)(N\geq 1)$ aircraft and present the relative kinematics for the AFF system involving a referential aircraft (RA) and follower aircraft $1,\ldots,N$, where N is a given positive integer. The origin of coordinates frame for the fleet is attached to the c.g. of the RA. The relative kinematics models the relative position and orientation of the follower aircraft i in the formation with respect to the RA.

We use $F_E(o_E, x_E, y_E, z_E)$ to denote an inertial system, which is attached to the Earth, and its origin o_E is located to one point on ground. Here, we assume that the Earth is flat and nonrotating. F_E is a right-handed reference system, the axis $o_E x_E$ is horizontal and points to North, and the axis $o_E y_E$ and $o_E z_E$ are horizontally East and vertically downward, respectively. Let $F_{W_i}(o_i, x_i, y_i, z_i)$, $i=0,1,\ldots,N+1$ denote the wind reference frame. Each wind frame is fixed to the center of gravity of the aircraft i and moves with it. This is also a right-handed orthogonal frame system, the axis $o_i x_i$ is aligned with the velocity vector of the aircraft i, the axis $o_i y_i$ points to the right wing, and the axis $o_i z_i$ points towards the bottom of the aircraft i. Let a set of coordinate charts given by x_i, y_i, z_i, ϕ_i, ψ_i, θ_i represent the position and orientation of the aircraft i, where ϕ_i, ψ_i, θ_i are Euler angles, that is, roll, yaw, and pitch angles, respectively. The definitions for the inertial and wind coordinate systems as well as the Euler angles are depicted in Fig. 1.

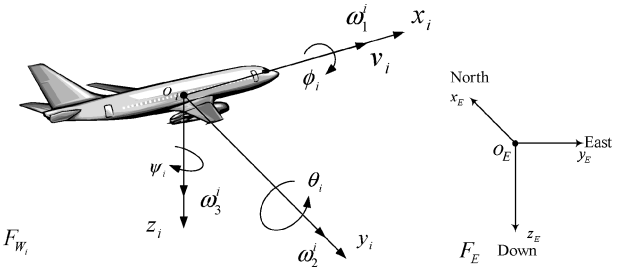

Fig. 1 Definitions for the inertial and wind coordinates systems.

For the three-dimensional flight the configuration of an individual aircraft can be treated as one element of the Lie group $\mathbb{G}$ of rigid motions in $\mathbb{R}^3$, known as $SE(3)$. Here SE stands for the special Euclidean group. Let $g_0, g_i \in \mathbb{G}$ denote the configurations of the RA and the aircraft i $(i>0)$ in the formation, respectively. Let $g_{\mathrm{ri}} \in \mathbb{G}$ denote the relative configuration of the aircraft i with respect to the RA. If the trajectories of both aircraft are modelled as left invariant vector fields on the Lie group $\mathbb{G}$, the relative kinematics of configuration is as follows[14–16]:

$$\begin{aligned}\dot{g}_{\mathrm{ri}} &= g_{\mathrm{ri}}\chi_i - \chi_0 g_{\mathrm{ri}} = g_{\mathrm{ri}}\chi_i - g_{\mathrm{ri}}g_{\mathrm{ri}}^{-1}\chi_0 g_{\mathrm{ri}} \\ &= g_{\mathrm{ri}}\chi_i - g_{\mathrm{ri}}Ad_{g_{\mathrm{ri}}^{-1}}\chi_0 = g_{\mathrm{ri}}\left[\chi_i - Ad_{g_{\mathrm{ri}}^{-1}}\chi_0\right] \end{aligned} \tag{2}$$

where χ_0, $\chi_i \in \mathbb{G}$ are the Lie algebra associated with the Lie group $\mathbb{G}$ and $Ad_{g_{\mathrm{ri}}^{-1}}\chi_0 = g_{\mathrm{ri}}^{-1}\chi_0 g_{\mathrm{ri}} \in \mathbb{G}$.

In the Euclidean group $SE(3)$, g_{ri} and its associated Lie algebra element are of the following forms[15]:

$$\chi_j = \begin{bmatrix} 0 & -\omega_3^j & \omega_2^j & v_j \\ \omega_3^j & 0 & -\omega_1^j & 0 \\ -\omega_2^j & \omega_1^j & 0 & 0 \\ 0 & 0 & 0 & 0 \end{bmatrix}$$

$$g_{\mathrm{ri}} = \begin{bmatrix} \boldsymbol{A}_{i1} & \vdots & \boldsymbol{A}_{i2} \end{bmatrix}, \qquad j = 0, i \tag{3}$$

with

$$\boldsymbol{A}_{i1} = \begin{bmatrix} C\psi_{\mathrm{ri}}C\theta_{\mathrm{ri}} & C\psi_{\mathrm{ri}}S\theta_{\mathrm{ri}}S\phi_{\mathrm{ri}} - S\psi_{\mathrm{ri}}C\phi_{\mathrm{ri}} \\ S\psi_{\mathrm{ri}}C\theta_{\mathrm{ri}} & S\psi_{\mathrm{ri}}S\theta_{\mathrm{ri}}S\phi_{\mathrm{ri}} + C\psi_{\mathrm{ri}}C\phi_{\mathrm{ri}} \\ -S\theta_{\mathrm{ri}} & C\theta_{\mathrm{ri}}S\phi_{\mathrm{ri}} \\ 0 & 0 \end{bmatrix}$$

$$\boldsymbol{A}_{i2} = \begin{bmatrix} C\psi_{\mathrm{ri}}S\theta_{\mathrm{ri}}C\phi_{\mathrm{ri}} + S\psi_{\mathrm{ri}}S\phi_{\mathrm{ri}} & x_{\mathrm{ri}} \\ S\psi_{\mathrm{ri}}S\theta_{\mathrm{ri}}C\phi_{\mathrm{ri}} - C\psi_{\mathrm{ri}}S\phi_{\mathrm{ri}} & y_{\mathrm{ri}} \\ C\theta_{\mathrm{ri}}C\phi_{\mathrm{ri}} & z_{\mathrm{ri}} \\ 0 & 1 \end{bmatrix} \tag{4}$$

where C, S denote the cosine and sine of the related angle, respectively. After substitution of Eqs. (3) and (4) into Eq. (2), we can obtain the following relative kinematics model for the

three-dimensional AFF system[14,15]:

$$\dot{x}_{\mathrm{ri}} = -v_0 + \omega_3^0 y_{\mathrm{ri}} - \omega_2^0 z_{\mathrm{ri}} + v_i C\psi_{\mathrm{ri}} C\theta_{\mathrm{ri}}$$

$$\dot{y}_{\mathrm{ri}} = -\omega_3^0 x_{\mathrm{ri}} + \omega_1^0 z_{\mathrm{ri}} + v_i S\psi_{\mathrm{ri}} C\theta_{\mathrm{ri}}$$

$$\dot{z}_{\mathrm{ri}} = \omega_2^0 x_{\mathrm{ri}} - \omega_1^0 y_{\mathrm{ri}} - v_i S\theta_{\mathrm{ri}}$$

$$\dot{\phi}_{\mathrm{ri}} = \omega_1^i + (1/C\theta_{\mathrm{ri}})\left[\omega_3^i C\phi_{\mathrm{ri}} S\theta_{\mathrm{ri}} - \omega_2^0 S\psi_{\mathrm{ri}} - \omega_1^0 C\psi_{\mathrm{ri}} + \omega_2^i S\phi_{\mathrm{ri}} S\theta_{\mathrm{ri}}\right]$$

$$\dot{\psi}_{\mathrm{ri}} = -\omega_3^0 + (1/C\theta_{\mathrm{ri}})\left[-\omega_2^0 S\psi_{\mathrm{ri}} S\theta_{\mathrm{ri}} + \omega_2^i S\phi_{\mathrm{ri}} + \omega_3^i C\phi_{\mathrm{ri}} - \omega_1^0 C\psi_{\mathrm{ri}} S\theta_{\mathrm{ri}}\right]$$

$$\dot{\theta}_{\mathrm{ri}} = -\omega_2^0 C\psi_{\mathrm{ri}} + \omega_2^i C\phi_{\mathrm{ri}} + \omega_1^0 S\psi_{\mathrm{ri}} - \omega_3^i S\phi_{\mathrm{ri}} \tag{5}$$

The sign of the second term $\omega_3^0\, y_{\mathrm{ri}}$ of the first equation in Eq. (5) should be positive rather than negative in Refs. 14 and 15. Moreover, the model described by Eq. (5) will be posed ill condition if $\theta_{\mathrm{ri}} = \pm\pi/2$ as expected from the singularity of the roll-yaw-pitch parameterization of $SE(3)$. Therefore, this flight condition should be avoided for the three-dimensional autonomous formation. In this study we confine our attention only to a limited range of the relative orientation for the sake of simplicity, namely, $|\phi_{\mathrm{ri}}| \le 2\pi$, $|\psi_{\mathrm{ri}}| \le 2\pi$, $|\theta_{\mathrm{ri}}| < \pi/2$.

III. Problem Statement

Having established the full relative kinematics, in this section we formulate the control problem for the three-dimensional formation flight of $N+1 (N \ge 1)$ aircraft as shown in Fig. 2. To facilitate the control development, we first rearrange the nonlinear relative kinematics of the AFF system into the following multi-input/multi-output (MIMO) nonlinear affine control system with a drift term, that is,

$$\dot{\boldsymbol{x}} = \boldsymbol{f}(\boldsymbol{x}) + \boldsymbol{g}(\boldsymbol{x})\boldsymbol{u}, \qquad \boldsymbol{y} = \boldsymbol{h}(\boldsymbol{x}) \tag{6}$$

where $\boldsymbol{x} = (x_{\mathrm{ri}},\ y_{\mathrm{ri}},\ z_{\mathrm{ri}},\ \phi_{\mathrm{ri}},\ \psi_{\mathrm{ri}},\ \theta_{\mathrm{ri}})^T \in \mathbb{M}_0 \subset \mathbb{R}^6$, $\mathbb{M}_0$ is a real analytic manifold and defined by $\mathbb{M}_0 := \{(x_{\mathrm{ri}}, y_{\mathrm{ri}}, z_{\mathrm{ri}}, \phi_{\mathrm{ri}}, \psi_{\mathrm{ri}}, \theta_{\mathrm{ri}}) | (x_{\mathrm{ri}} - x_{\mathrm{ri}}^d)^2 + (y_{\mathrm{ri}} - y_{\mathrm{ri}}^d)^2 + (z_{\mathrm{ri}} - z_{\mathrm{ri}}^d)^2 \le R_i^2,\ |\phi_{\mathrm{ri}}| \le 2\pi,\ |\psi_{\mathrm{ri}}| \le 2\pi, |\theta_{\mathrm{ri}}| < \pi/2\}$. $\boldsymbol{u} = (v_i, \omega_1^i, \omega_2^i, \omega_3^i)^T$ is the input vector within the admissible control set $\Omega := \{(v_i, \omega_1^i, \omega_2^i, \omega_3^i) | 0 < v_i \le \bar{v}_i, |\omega_1^i| \le \bar{\omega}_1^i, |\omega_2^i| \le \bar{\omega}_2^i, |\omega_3^i| \le \bar{\omega}_3^i\}$. $f(x)$, $\boldsymbol{g}(\boldsymbol{x}) = [\boldsymbol{g}_1(\boldsymbol{x}), \boldsymbol{g}_2(\boldsymbol{x}), \boldsymbol{g}_3(\boldsymbol{x}), \boldsymbol{g}_4(\boldsymbol{x})]$ are smooth vector fields, and $\boldsymbol{h}(\boldsymbol{x}) = [h_1(\boldsymbol{x}), h_2(\boldsymbol{x}), h_3(\boldsymbol{x}), h_4(\boldsymbol{x})]^T$ is a smooth vector function defined on $\mathbb{M}_0$:

$$\boldsymbol{f}(\boldsymbol{x}) = \begin{pmatrix} -v_0 + \omega_3^0 y_{\mathrm{ri}} - \omega_2^0 z_{\mathrm{ri}} \\ -\omega_3^0 x_{\mathrm{ri}} + \omega_1^0 z_{\mathrm{ri}} \\ \omega_2^0 x_{\mathrm{ri}} - \omega_1^0 y_{\mathrm{ri}} \\ -\omega_2^0 \sec\theta_{\mathrm{ri}} \sin\psi_{\mathrm{ri}} - \omega_1^0 \cos\psi_{\mathrm{ri}} \sec\theta_{\mathrm{ri}} \\ -\omega_3^0 - \omega_2^0 S\psi_{\mathrm{ri}} \tan\theta_{\mathrm{ri}} - \omega_1^0 C\psi_{\mathrm{ri}} \tan\theta_{\mathrm{ri}} \\ -\omega_2^0 \cos\psi_{\mathrm{ri}} + \omega_1^0 \sin\psi_{\mathrm{ri}} \end{pmatrix}$$

$$\boldsymbol{g}(\boldsymbol{x}) = \begin{pmatrix} C\psi_{\mathrm{ri}} C\theta_{\mathrm{ri}} & 0 & 0 & 0 \\ S\psi_{\mathrm{ri}} C\theta_{\mathrm{ri}} & 0 & 0 & 0 \\ -\sin\theta_{\mathrm{ri}} & 0 & 0 & 0 \\ 0 & 1 & S\phi_{\mathrm{ri}} \tan\theta_{\mathrm{ri}} & C\phi_{\mathrm{ri}} \tan\theta_{\mathrm{ri}} \\ 0 & 0 & S\phi_{\mathrm{ri}} \sec\theta_{\mathrm{ri}} & C\phi_{\mathrm{ri}} \sec\theta_{\mathrm{ri}} \\ 0 & 0 & \cos\phi_{\mathrm{ri}} & -\sin\phi_{\mathrm{ri}} \end{pmatrix}$$

$$\boldsymbol{h}(\boldsymbol{x}) = \left(x_{\mathrm{ri}} - x_{\mathrm{ri}}^d,\ y_{\mathrm{ri}} - y_{\mathrm{ri}}^d,\ z_{\mathrm{ri}} - z_{\mathrm{ri}}^d,\ \phi_{\mathrm{ri}} - \phi_{\mathrm{ri}}^d\right)^T \tag{7}$$

where $(x_{\mathrm{ri}}^d, y_{\mathrm{ri}}^d, z_{\mathrm{ri}}^d)^T$ and ϕ_{ri}^d are the desired relative position vector and roll angle, respectively.

In this work we assume that each aircraft i has an ideal inner-loop controller by which the required control inputs $(v_i, \omega_1^i, \omega_2^i, \omega_3^i)^T$ can be available for the formation control level. Because we do not require any detailed information on specific aircraft, such as structure sizes, aerodynamics, propulsive power, flight conditions, and so on, the controllers obtained for the AFF system will be only kinematics dependent.

Next, let $\boldsymbol{q}_i(t) = [x_{\mathrm{ri}}(t), y_{\mathrm{ri}}(t), z_{\mathrm{ri}}(t)]^T$ and $\boldsymbol{q}_i^d(t) = (x_{\mathrm{ri}}^d, y_{\mathrm{ri}}^d, z_{\mathrm{ri}}^d)^T$ denote the actual and desired relative position vector with respect to the RA, respectively. To quantify the effectiveness of the control objective, we define a distance $d_i(t)$ between $\boldsymbol{q}_i(t)$ and $\boldsymbol{q}_i^d$ as the following form:

$$d_i(t) = \sqrt{\left[x_{\mathrm{ri}}(t) - x_{\mathrm{ri}}^d\right]^2 + \left[y_{\mathrm{ri}}(t) - y_{\mathrm{ri}}^d\right]^2 + \left[z_{\mathrm{ri}}(t) - z_{\mathrm{ri}}^d\right]^2} \tag{8}$$

In the following, let $A_i(v_i, \omega_1^i, \omega_2^i, \omega_3^i)$ denote the set of the velocities of the aircraft $i, i = 0, 1, \ldots, N+1$. Now, we can formulate the control problem for the AFF system under consideration in this paper as follows:

Problem 1 (formation-keeping control): Consider the AFF system of $N+1 (N \ge 1)$ aircraft in three-dimensional space. The formation geometry of the follower aircraft $i (i > 0)$ and the RA is shown as in Fig. 2. Assume that the motion state $A_0(v_0, \omega_1^0, \omega_2^0, \omega_3^0)$ of the RA is time invariant during the regulation process of the follower aircraft i.

Given a desired, constant relative position $\boldsymbol{q}_i^d$ for the follower aircraft i with respect to the RA, design a relative position-keeping controller $\boldsymbol{u}$ for the system described by Eq. (6) such that the follower aircraft i is forced from an initial position $q_i(0)$ to the desired relative position $\boldsymbol{q}_i^d$ as $t \to \infty$, that is,

$$\lim_{t \to \infty} d_i(t) = 0 \tag{9}$$

Remark 1: In Problem 1 it is assumed that the motion state $A_0(v_0, \omega_1^0, \omega_2^0, \omega_3^0)$ of the RA can be kept as constant during the formation-keeping control of the aircraft i. Although this assumption seems somewhat fastidious, it could be acceptable in the practice of autonomous formation flight, in particular, cruise formation flight. In this case the motion of the RA can be designed to be held as constant in each phase or flight mode of formation flying. On the other hand, the desirable motion state $A_0(v_0, \omega_1^0, \omega_2^0, \omega_3^0)$ can be flexibly designed in terms of the flight tasks when a virtual aircraft is designated as a referential aircraft. Hence, the results of this study will be particularly effective to the formation-keeping control of virtual leader-based formation flight of multiple aircraft.

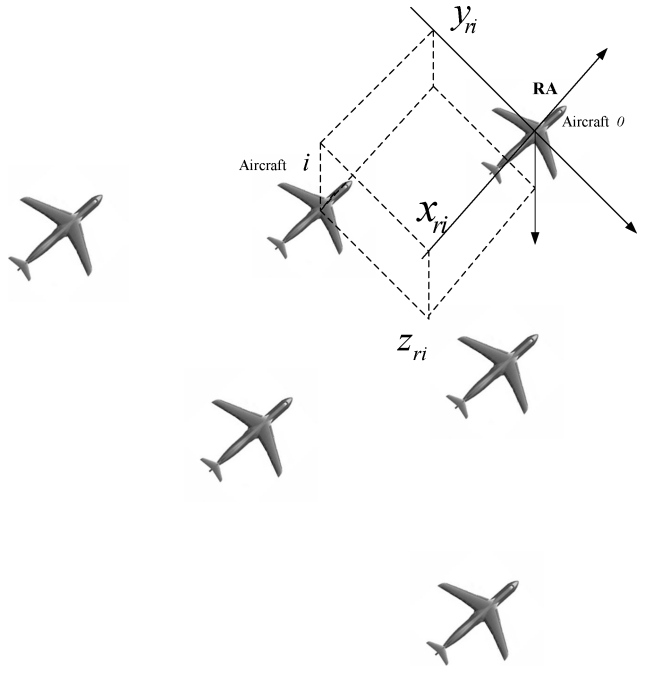

Fig. 2 Schematic drawing for the AFF system.

Let $\boldsymbol{\sigma} = \{\sigma_1, \ldots, \sigma_m\}$ denote the vector relative degree. The $m \times m$ decoupling matrix is defined by

$$\boldsymbol{\rho}(\boldsymbol{x}) = \left[L_{g_j} L_f^{\sigma_k - 1} h_k(\boldsymbol{x})\right]_{m \times m}, \qquad j, k = 1, \ldots, m \tag{10}$$

As is known, if the relative degree $\boldsymbol{\sigma}$ is well defined at some point x_0 on a dense open manifold, the decoupling matrix $\boldsymbol{\rho}(\boldsymbol{x})$ must be nonsingular.[17] With the preceding discussion we conclude that the system of Eq. (6) possesses the following property:

Property 1 (Singularity):

1) The decoupling matrix $\boldsymbol{\rho}(\boldsymbol{x})$ of the nonlinear control system (6) is singular.

2) For the system (6) there does not exist a regular static state feedback and a local change of coordinate $\boldsymbol{\xi} = \boldsymbol{\Phi}(\boldsymbol{x})$ to directly transform it into a controllable linear system from the sense of input-output (static) feedback linearization in the state space.

Proof: Differentiating the output y of Eq. (6) once with respect to time, one can find that all the inputs u_i, $i = 1, \ldots, 4$ already appear in $\dot{\boldsymbol{y}}$. Thus, we can obtain the decoupling matrix as

$$\boldsymbol{\rho}(\boldsymbol{x}) = \begin{bmatrix} C\psi_{\mathrm{ri}} C\theta_{\mathrm{ri}} & 0 & 0 & 0 \\ C\theta_{\mathrm{ri}} S\psi_{\mathrm{ri}} & 0 & 0 & 0 \\ -S\theta_{\mathrm{ri}} & 0 & 0 & 0 \\ 0 & 1 & S\phi_{\mathrm{ri}} \tan\theta_{\mathrm{ri}} & C\phi_{\mathrm{ri}} \tan\theta_{\mathrm{ri}} \end{bmatrix}$$

Because $\mathrm{Rank}[\boldsymbol{\rho}(\boldsymbol{x})] = 2$ everywhere on the manifold $\mathbb{M}_0$, the decoupling matrix is singular. Hence, a well-defined definition for the vector relative degree $\boldsymbol{\sigma}$ does not exist for system (6).[17] This fact shows that there does not exist a regular (static) state feedback and a local coordinates transformation $\boldsymbol{\xi} = \boldsymbol{\Phi}(\boldsymbol{x})$ to directly transform system (6) into an exact linearized form via static feedback from the viewpoint of input-output feedback linearization.[17] □

According to Property 1, the control design based on input–output (static feedback) linearization to an exact linearized or a partial linearized form will break down. As such, the ordinary output tracking methods based on NDI, such as in Refs. 13 and 17, will fail to give a control solution to Problem 1 because they always require that the system must have a well-defined (vector) relative degree.

Because the relative degree is invariant under static-state feedback, one cannot transform the original system described by Eq. (6), which does not have a well-defined relative degree into a new system that does have a well-defined relative degree by means of static-state feedback. Thus, to achieve a well-defined relative degree usually one can choose the dynamic extension method, which is realized by augmenting the dynamical equations with integrators added at the input channels.[18] However, some auxiliary state variables will be introduced during the process of dynamic extension.[18] As shown in Ref. 18, the dynamic extensions for input v_i and ω_1^i are needed to achieve a well-defined vector relative degree. As such, one must incorporate some dynamics relating to v_i and ω_1^i into the considered system, and the system will be augmented by using v_i and ω_1^i as two auxiliary state variables. If the objective of system design is not restricted to derive a generic formation-keeping control law that only depends on the relative kinematics of formation flight, then dynamic extension strategy is also an ideal option to solve the singular problem of decoupling matrix.

To deal with the singularity of decoupling matrix, one alternative approach is to utilize the nonlinear dynamic invertibility of system.[19] The advantage of using NDI is that we do not need to augment the original system and introduce the auxiliary state variables. As such, for the problem under consideration in this study a full kinematics-dependent control law can be established. The basic tool for constructing a nonlinear dynamic inversion is the well-known structure algorithm introduced by Hirschorn[20] and Singh.[21,22] However, for system (6) one can find that the structure algorithm will also fail to yield a nonlinear dynamic inversion. To check this negative result, one can resort to the tool package provided by Ref. 19.

To overcome the aforementioned difficulties of the system under consideration, a dual-controller approach is proposed in this study. In contrast to Ref. 18, this novel method does not require dynamically augmenting the original system of Eq. (6).

IV. System Decomposition

Analyzing the details of Eq. (6), we find that the second control input u_2 only exists in the fourth subequation and the state ϕ_{ri} is only in the fourth output y_4. Hence, we can decompose the original system (6) into the following two subsystems.

A. Subsystem I

$$\dot{\tilde{\boldsymbol{x}}} = \tilde{\boldsymbol{f}}(\tilde{\boldsymbol{x}}) + \tilde{\boldsymbol{g}}(\tilde{\boldsymbol{x}})\tilde{\boldsymbol{u}}, \qquad \tilde{\boldsymbol{y}} = \tilde{\boldsymbol{h}}(\tilde{\boldsymbol{x}}) \tag{11}$$

where $\tilde{\boldsymbol{x}} = (x_{\mathrm{ri}}, y_{\mathrm{ri}}, z_{\mathrm{ri}}, \psi_{\mathrm{ri}}, \theta_{\mathrm{ri}})^T \in \tilde{\mathbb{M}}_0 \subset \mathbb{R}^5$, $\tilde{\mathbb{M}}_0$ is defined by $\tilde{\mathbb{M}}_0 := \{(x_{\mathrm{ri}}, y_{\mathrm{ri}}, z_{\mathrm{ri}}, \psi_{\mathrm{ri}}, \theta_{\mathrm{ri}}) |\ (x_{\mathrm{ri}} - x_{\mathrm{ri}}^d)^2 + (y_{\mathrm{ri}} - y_{\mathrm{ri}}^d)^2 + (z_{\mathrm{ri}} - z_{\mathrm{ri}}^d)^2 \le R_i^2,\ |\psi_{\mathrm{ri}}| \le 2\pi,\ |\theta_{\mathrm{ri}}| < \pi/2\}$. $\tilde{\boldsymbol{y}} = (y_1, y_2, y_3)^T$, $\tilde{u} = (u_1, u_3, u_4)^T$ belongs to the admissible control set $\tilde{\Omega} := \{(v_i, \omega_2^i, \omega_3^i) | 0 < v_i \le \bar{v}_i,\ |\omega_2^i| \le \bar{\omega}_2^i,\ |\omega_3^i| \le \bar{\omega}_3^i\}$. Obviously, the subsystem I of Eq. (11) is also a square MIMO affine control system. In Eq. (11), $\tilde{\boldsymbol{f}}(\tilde{\boldsymbol{x}})$, $\tilde{\boldsymbol{g}}(\tilde{\boldsymbol{x}})$ are the smooth vector fields, and $\tilde{\boldsymbol{h}}(\boldsymbol{x}) = [h_1(\tilde{\boldsymbol{x}}), h_2(\tilde{\boldsymbol{x}}), h_3(\tilde{\boldsymbol{x}})]^T$ is a smooth vector function defined by

$$\tilde{\boldsymbol{f}}(\tilde{\boldsymbol{x}}) = \begin{pmatrix} -v_0 + \omega_3^0 y_{\mathrm{ri}} - \omega_2^0 z_{\mathrm{ri}} \\ -\omega_3^0 x_{\mathrm{ri}} + \omega_1^0 z_{\mathrm{ri}} \\ \omega_2^0 x_{\mathrm{ri}} - \omega_1^0 y_{\mathrm{ri}} \\ -\omega_3^0 - \omega_2^0 S\psi_{\mathrm{ri}} \tan\theta_{\mathrm{ri}} - \omega_1^0 C\psi_{\mathrm{ri}} \tan\theta_{\mathrm{ri}} \\ -\omega_2^0 C\psi_{\mathrm{ri}} + \omega_1^0 S\psi_{\mathrm{ri}} \end{pmatrix}$$

$$\tilde{\boldsymbol{g}}(\tilde{\boldsymbol{x}}) = \begin{pmatrix} C\psi_{\mathrm{ri}} C\theta_{\mathrm{ri}} & 0 & 0 \\ S\psi_{\mathrm{ri}} C\theta_{\mathrm{ri}} & 0 & 0 \\ -\sin\theta_{\mathrm{ri}} & 0 & 0 \\ 0 & S\phi_{\mathrm{ri}} \sec\theta_{\mathrm{ri}} & C\phi_{\mathrm{ri}} \sec\theta_{\mathrm{ri}} \\ 0 & \cos\phi_{\mathrm{ri}} & -\sin\phi_{\mathrm{ri}} \end{pmatrix}$$

$$\tilde{\boldsymbol{h}}(\tilde{\boldsymbol{x}}) = \left(x_{\mathrm{ri}} - x_{\mathrm{ri}}^d, y_{\mathrm{ri}} - y_{\mathrm{ri}}^d, z_{\mathrm{ri}} - z_{\mathrm{ri}}^d\right)^T \tag{12}$$

respectively.

B. Subsystem II

The second subsystem is formulated as follows:

$$\dot{\phi}_{\mathrm{ri}} = -\omega_2^0 \sec\theta_{\mathrm{ri}} \sin\psi_{\mathrm{ri}} - \omega_1^0 \cos\psi_{\mathrm{ri}} \sec\theta_{\mathrm{ri}} + u_2 + u_3 \sin\phi_{\mathrm{ri}} \tan\theta_{\mathrm{ri}} + u_4 \cos\phi_{\mathrm{ri}} \tan\theta_{\mathrm{ri}}$$

$$y_4 = \phi_{\mathrm{ri}} - \phi_{\mathrm{ri}}^d \tag{13}$$

In a formation flight problem we are particularly interested in transient effects because they are more critical to avoid possible collisions among the participating aircraft in the fleet and obtain the desirable performance of formation keeping or reconfiguration. One solution to obtain the desirable transient effects is the use of the output-tracking control scheme. For instance, we would expect that the followers could be forced to their desired relative positions exponentially by tracking some reference signal with an exponential convergence rate. In addition, the output tracking would also provide some reasonable and acceptable estimations on the bounds of separation errors during the transients of formation flying. Therefore, we will design an output-tracking controller for the subsystem I to follow the reference input $\tilde{\boldsymbol{y}}_R(t)$. Correspondingly, a $\phi_{\mathrm{ri}} -$ hold controller can be developed for the subsystem II such that the relative roll angle ϕ_{ri} converges to a desired relative roll angle ϕ_{ri}^d as time increases. Obviously, this is a dual-controller approach to problem 1, which will be treated in detail in the following sections.

Here, although one can prove that the subsystem I still possesses a similar property as stated in property 1, now a nonlinear dynamic inverse for the subsystem I can be constructed via the structure algorithm (see the following section for the details).

V. Output-Tracking Controller

To analyze the invertibility of the subsystem I, the following notion is first introduced into this study[19–22]:

Definition 1(Invertible): Given a smooth nonlinear affine control system:

$$\dot{\boldsymbol{x}} = \boldsymbol{f}(\boldsymbol{x}) + [\boldsymbol{g}_1(\boldsymbol{x}), \ldots, \boldsymbol{g}_m(\boldsymbol{x})]\,\boldsymbol{u} := \boldsymbol{f}(\boldsymbol{x}) + \boldsymbol{g}(\boldsymbol{x})\boldsymbol{u}$$

$$\boldsymbol{y} = (h_1(\boldsymbol{x}), \ldots, h_p(\boldsymbol{x}))^T := \boldsymbol{h}(\boldsymbol{x}) \tag{14}$$

where $\boldsymbol{x} \in \mathbb{M} \subset \mathbb{R}^n$, $\mathbb{M}$ is a real analytic manifold, $y = (y_1, \ldots, y_p) \in \mathbb{R}^p$, $\boldsymbol{u} = (u_1, \ldots, u_m) \in \mathbb{R}^m$. $\boldsymbol{f}(\boldsymbol{x})$, $\boldsymbol{g}_1(\boldsymbol{x}), \ldots, \boldsymbol{g}_m(\boldsymbol{x})$ are smooth vector fields, and $h_1(\boldsymbol{x}), \ldots, h_p(\boldsymbol{x})$ are smooth functions defined on an open set of $\mathbb{M}$.

1) The system (14) is invertible at $\boldsymbol{x}_0 \in \mathbb{M}$ if whenever $\boldsymbol{u}_1(t)$ and $\boldsymbol{u}_2(t)$ are distinct admissible (real, analytic) controls, $\boldsymbol{y}(\cdot, \boldsymbol{u}_1, \boldsymbol{x}_0) \neq \boldsymbol{y}(\cdot, \boldsymbol{u}_2, \boldsymbol{x}_0)$.

2) The system (14) is strongly invertible at $\boldsymbol{x}_0 \in \mathbb{M}$ if the system is invertible at each $x \in \mathbb{V}$, where $\mathbb{V}$ is an open neighborhood of $\boldsymbol{x}_0$.

3) The system (14) is strongly invertible if there exists an open and dense submanifold $\tilde{\mathbb{M}}$ of $\mathbb{M}$ such that for all $\boldsymbol{x}_0 \in \tilde{\mathbb{M}}$ the system is strongly invertible at $\boldsymbol{x}_0$.

A. Invertibility Analysis

For the subsystem I, according to the preceding definition of invertibility, we have the following proposition:

Proposition 1: The relative order α of the subsystem I is finite, that is, $\alpha < \infty$. Thus, there exists an open dense submanifold $\mathbb{M}_\alpha \subset \tilde{\mathbb{M}}_0$ such that the subsystem I is strongly invertible at $\tilde{\boldsymbol{x}}_0$ for all $\tilde{\boldsymbol{x}}_0 \in \mathbb{M}_\alpha$

Proof: Following the structure algorithm outlined in Appendix A, the proof is straightforward. Here, ϕ_{ri} is treated as a time-varying variable during the following procedure.

Beginning with Eq. (11), the system 1 in the structure algorithm has the following form:

$$\dot{\tilde{\boldsymbol{x}}} = \tilde{\boldsymbol{f}}(\tilde{\boldsymbol{x}}) + \tilde{\boldsymbol{g}}(\tilde{\boldsymbol{x}})\tilde{\boldsymbol{u}}$$

$$z_1 = (\bar{z}_1, \hat{z}_1)^T = \begin{bmatrix} -v_0 + \omega_3^0 y_{\mathrm{ri}} - \omega_2^0 z_{\mathrm{ri}} \\ -\omega_3^0 x_{\mathrm{ri}} + \omega_1^0 z_{\mathrm{ri}} - D_1^* \tan\psi_{\mathrm{ri}} \\ \omega_2^0 x_{\mathrm{ri}} - \omega_1^0 y_{\mathrm{ri}} + D_1^* \sec\psi_{\mathrm{ri}} \tan\theta_{\mathrm{ri}} \end{bmatrix} + \begin{bmatrix} \cos\psi_{\mathrm{ri}}\cos\theta_{\mathrm{ri}} & 0 & 0 \\ 0 & 0 & 0 \\ 0 & 0 & 0 \end{bmatrix} \tilde{\boldsymbol{u}}$$

$$\hat{z}_1 = \begin{bmatrix} -\tan\psi_{\mathrm{ri}}\dot{y}_1 + \dot{y}_2 \\ \sec\psi_{\mathrm{ri}}\tan\theta_{\mathrm{ri}}\dot{y}_1 + \dot{y}_3 \end{bmatrix}$$

Obviously, one gets $r_1 = 1$. $\mathbb{M}_1$ can be constructed as

$$\mathbb{M}_1 := \{\tilde{\boldsymbol{x}} \in \tilde{\mathbb{M}}_0 | \cos\psi_{\mathrm{ri}} \neq 0\}$$

Differentiating $\hat{z}_1$ to obtain the system 2 as follows,

$$\dot{\tilde{\boldsymbol{x}}} = \tilde{\boldsymbol{f}}(\tilde{\boldsymbol{x}}) + \tilde{\boldsymbol{g}}(\tilde{\boldsymbol{x}})\tilde{\boldsymbol{u}}$$

$$z_2 = \begin{pmatrix} \bar{z}_2 \\ \hat{z}_2 \end{pmatrix} = \begin{pmatrix} D_1^* \\ c_{21} \\ c_{31} \end{pmatrix} + \boldsymbol{D}_2((\tilde{\boldsymbol{x}}, \dot{\tilde{\boldsymbol{y}}}))\tilde{\boldsymbol{u}}$$

in which

$$\boldsymbol{D}_2[(\tilde{\boldsymbol{x}}, \dot{\tilde{\boldsymbol{y}}})] = \begin{pmatrix} \cos\psi_{\mathrm{ri}}\cos\theta_{\mathrm{ri}} & 0 & 0 \\ d_{21} & d_{22} & d_{23} \\ d_{31} & d_{32} & d_{33} \end{pmatrix}$$

where $c_{21}, c_{31}, d_{jk}\,(j = 2, 3;\ k = 1, 2, 3)$ are the interim symbols and are listed in Appendix B.

Because $\det\{\boldsymbol{D}_2[(\tilde{\boldsymbol{x}}, \dot{\tilde{\boldsymbol{y}}})]\} = \sec^2\psi_{\mathrm{ri}}\sec^2\theta_{\mathrm{ri}} D_2^{*2}$, we can construct submanifold $\mathbb{M}_2$ to satisfy $\mathbb{M}_2 \times \mathbb{Y}_1^1 := \{(\tilde{\boldsymbol{x}}, \dot{\tilde{\boldsymbol{y}}}) | \tilde{x} \in \mathbb{M}_1,\ \dot{\tilde{\boldsymbol{y}}} \in \mathbb{Y}_1 = \mathbb{R}^3$ with $D_2^* \neq 0$, that is, $\dot{y}_1 \neq -v_0 + \omega_3^0 y_{\mathrm{ri}} - \omega_2^0 z_{\mathrm{ri}}\}$. As such, it is shown that the rank of $\boldsymbol{D}_2((\tilde{\boldsymbol{x}}, \dot{\tilde{\boldsymbol{y}}}))$ is 3, and its inverse is well-defined everywhere on the submanifold $\mathbb{M}_2$. Owing to $r_2 = 3 = \min(m, p) = m$, the relative order α of the subsystem I is 2. According to definition 1 and theorem 2 in Ref. 22, the subsystem I is strongly invertible at $\tilde{\boldsymbol{x}}_0$ for all $\tilde{\boldsymbol{x}}_0 \in \mathbb{M}_\alpha$.

We note that $\mathbb{Y}_1^1 \neq \mathbb{R}^3$. However, $\mathbb{Y}_1^1$ is characterized by the following condition:

$$\dot{y}_1 \neq -v_0 + \omega_3^0 y_{\mathrm{ri}} - \omega_2^0 z_{\mathrm{ri}}$$

Owing to $\dot{y}_1 = -v_0 + \omega_3^0 y_{\mathrm{ri}} - \omega_2^0 z_{\mathrm{ri}} + v_i \cos\psi_{\mathrm{ri}} \cos\theta_{\mathrm{ri}}$, the preceding condition yields that the input $v_i \neq 0$ for all $\tilde{\boldsymbol{x}} \in \mathbb{M}_1$. Because the speed of each participating aircraft in the fleet is always assumed to be nonzero, the condition $v_i \neq 0$ consequentially holds for the formation flight case of multiple aircraft. □

Proposition 1 indicates that the subsystem I is of strong invertibility at $\tilde{\boldsymbol{x}}_0$ for all $\tilde{\boldsymbol{x}}_0 \in \mathbb{M}_\alpha = \mathbb{M}_2$. Consequently, the nonlinear dynamic inversion does exist on this submanifold. Then, in the following we turn to the construction of NDI and design a NDI-based output-tracking controller for the subsystem I by following the lines in Ref. 19.

B. Construction of NDI System

Generally speaking, the application of the structure algorithm will lead to a finite integer α and matrices $H_\alpha, C_\alpha, D_\alpha$ such that[19]

$$\boldsymbol{Z}_\alpha = \boldsymbol{H}_\alpha(\tilde{\boldsymbol{x}})\boldsymbol{Y}_\alpha(t) = \boldsymbol{C}_\alpha(\tilde{\boldsymbol{x}}) + \boldsymbol{D}_\alpha(\tilde{\boldsymbol{x}})\tilde{\boldsymbol{u}} \tag{15}$$

where $\boldsymbol{Y}_\alpha(\boldsymbol{t}) = [\dot{\tilde{\boldsymbol{y}}}^T, \ddot{\tilde{\boldsymbol{y}}}^T, \ldots \tilde{\boldsymbol{y}}^{(\alpha)^T}]^T$ and $\boldsymbol{D}_\alpha(\tilde{\boldsymbol{x}})$ is a $p \times m$ matrix with rank $\min(m, p)$. For the subsystem I we have obtained $\alpha = 2$ and $p = m = 3$, which follows that $\boldsymbol{D}_\alpha(\tilde{\boldsymbol{x}})$ has a right inverse the same as a left inverse $\boldsymbol{D}_\alpha^\dagger(\tilde{\boldsymbol{x}})$. Consequently, the system inverse is defined by

$$\dot{\tilde{\boldsymbol{x}}} = \tilde{\boldsymbol{f}}(\boldsymbol{x}) + \tilde{\boldsymbol{g}}(\tilde{\boldsymbol{x}})\tilde{\boldsymbol{u}}, \qquad \tilde{\boldsymbol{u}} = \boldsymbol{D}_\alpha^\dagger(\tilde{\boldsymbol{x}})\{-\boldsymbol{C}_\alpha(\tilde{\boldsymbol{x}}) + \boldsymbol{H}_\alpha(\tilde{\boldsymbol{x}})\boldsymbol{Y}_\alpha(t)\} \tag{16}$$

with

$$\boldsymbol{D}_\alpha(\tilde{\boldsymbol{x}}) = \boldsymbol{D}_2[(\tilde{\boldsymbol{x}}, \dot{\tilde{\boldsymbol{y}}})]$$

$$\boldsymbol{D}_\alpha^\dagger(\tilde{\boldsymbol{x}}) = \begin{bmatrix} \sec\psi_{\mathrm{ri}}\sec\theta_{\mathrm{ri}} & 0 & 0 \\ d_{21}^\alpha & d_{22}^\alpha & d_{23}^\alpha \\ d_{31}^\alpha & d_{32}^\alpha & d_{33}^\alpha \end{bmatrix}$$

$$\boldsymbol{C}_\alpha(\tilde{\boldsymbol{x}}) = \left(D_1^*, c_{21}, c_{31}\right)^T$$

$$\boldsymbol{H}_\alpha(\tilde{\boldsymbol{x}}) = \begin{bmatrix} 1 & 0 & 0 & 0 & 0 & 0 \\ H_{21} & 0 & 0 & -\tan\psi_{\mathrm{ri}} & 1 & 0 \\ H_{31} & 0 & 0 & \sec\psi_{\mathrm{ri}}\tan\theta_{\mathrm{ri}} & 0 & 1 \end{bmatrix}$$

$$\boldsymbol{Y}_\alpha(\boldsymbol{t}) = (\dot{y}_1, \dot{y}_2, \dot{y}_3, \ddot{y}_1, \ddot{y}_2, \ddot{y}_3)^T$$

$$\boldsymbol{Z}_\alpha = (\dot{y}_1, -\tan\psi_{\mathrm{ri}}\ddot{y}_1 + \ddot{y}_2, \sec\psi_{\mathrm{ri}}\tan\theta_{\mathrm{ri}}\ddot{y}_1 + \ddot{y}_3)^T$$

where the interim symbols H_{21}, H_{31}, d_{jk}^α $(j = 2, 3;\ k = 1, 2, 3)$ are also listed in Appendix B.

C. Tracking Control Law

Let us consider how to construct the output-tracking controller for the AFF system based on the inverse system of Eq. (16). Because not all of the elements in $\boldsymbol{Y}_\alpha$ actually survive multiplication by $\boldsymbol{H}_\alpha(\tilde{x})$ in Eq. (15), we can denote $\boldsymbol{H}_\alpha(\tilde{\boldsymbol{x}})\,\boldsymbol{Y}_\alpha = \tilde{\boldsymbol{H}}\tilde{\boldsymbol{Y}}$. Thus, Eq. (16) can be reassembled as the following form[19]:

$$\dot{\tilde{\boldsymbol{x}}} = \tilde{\boldsymbol{f}}(\tilde{\boldsymbol{x}}) + \tilde{\boldsymbol{g}}(\tilde{\boldsymbol{x}})\tilde{\boldsymbol{u}}, \qquad \tilde{\boldsymbol{u}} = \boldsymbol{D}_\alpha^\dagger(\tilde{\boldsymbol{x}})\{-\boldsymbol{C}_\alpha(\tilde{\boldsymbol{x}}) + \tilde{\boldsymbol{H}}\,\tilde{\boldsymbol{Y}}\} \tag{17}$$

In the following, let n_j and N_j $(j = 1, 2, 3)$ denote the lowest- and highest-order derivative of y_j appearing in $\boldsymbol{H}_\alpha(\boldsymbol{x})\boldsymbol{Y}_\alpha$, respectively. For the subsystem I one can find that $n_1 = 1, N_1 = 2, n_2 = 2, N_2 = 2, n_3 = 2, N_3 = 2$. Hence, we have

$$\tilde{\boldsymbol{H}} = \begin{bmatrix} 1 & 0 & 0 & 0 \\ 0 & -\tan\psi_{\mathrm{ri}} & 1 & 0 \\ 0 & \sec\psi_{\mathrm{ri}}\tan\theta_{\mathrm{ri}} & 0 & 1 \end{bmatrix}, \qquad \tilde{\boldsymbol{Y}} = (\dot{y}_1, \ddot{y}_1, \ddot{y}_2, \ddot{y}_3)^T$$

There are many approaches to design a tracking controller based on the concept of nonlinear dynamic inverse systems. In this study a perturbation controller based on the output tracking error[19] is utilized. If $\tilde{\boldsymbol{y}}_R(t)$ denotes the reference trajectory, then the feedforward control input will be taken as the following form:

$$\tilde{\boldsymbol{u}} = \boldsymbol{D}_\alpha^\dagger(\boldsymbol{x})\{-\boldsymbol{C}_\alpha(\boldsymbol{x}) + \tilde{\boldsymbol{H}}(x)\tilde{\boldsymbol{y}}_R(\boldsymbol{t}) + \boldsymbol{v}_p(\boldsymbol{t})\} \tag{18}$$

where $v_p(t)$ is the perturbation controller and chosen to be

$$v_{p,j} = \beta_{j,0}\int_0^t (\tilde{y}_{Rj} - y_j)dt + \sum_{k=0}^{n_j-1} w_{j,k}\left(\tilde{y}_{Rj}^{(k)} - y_j^{(k)}\right) \qquad j = 1, 2, 3 \tag{19}$$

Thus, if the following polynomials are Hurwitz,

$$\sum_{k=0}^{n_j+1} \beta_{j,k}\cdot s^k = 0, \qquad j = 1, 2, 3$$

$$\beta_{j,k} = w_{j,k-1}, \qquad k = 1, \ldots, n_j + 1 \tag{20}$$

then the stability of the closed-loop system can be guaranteed.[19]

VI. ϕ_{ri} – Hold Controller

In this section we deal with the design of relative roll angle-hold controller for the subsystem II. It is ready to establish the following result.

Proposition 2: Given a desired, constant roll angle ϕ_{ri}^d. Then, the continuous controller of the form

$$u_2 = \mu(\boldsymbol{x}, u_3, u_4) = \omega_2^0 \sec\theta_{\mathrm{ri}} \sin\psi_{\mathrm{ri}} + \omega_1^0 \cos\psi_{\mathrm{ri}} \sec\theta_{\mathrm{ri}} - u_3 \sin\phi_{\mathrm{ri}} \tan\theta_{\mathrm{ri}} - u_4 \cos\phi_{\mathrm{ri}} \tan\theta_{\mathrm{ri}} + K\left(\phi_{\mathrm{ri}}^d - \phi_{\mathrm{ri}}\right) \tag{21}$$

can stabilize the subsystem II exponentially for any initial state $\tilde{\boldsymbol{x}}(0) \in \mathbb{M}_2$ and $|\phi_{\mathrm{ri}}(0)| \le 2\pi$, that is, all of the solutions of the closed-loop system described by Eqs. (13) and (21) exponentially converge to ϕ_{ri}^d as $t \to \infty$, where K is a positive design parameter.

Proof: Substituting Eq. (21) into Eq. (13) yields the closed-loop system as

$$\dot{\phi}_{\mathrm{ri}} = K\left(\phi_{\mathrm{ri}}^d - \phi_{\mathrm{ri}}\right) \tag{22}$$

Thus, the error dynamics takes the following form:

$$\dot{e} + Ke = 0 \tag{23}$$

where the error is defined by $e := \phi_{\mathrm{ri}} - \phi_{\mathrm{ri}}^d$. It is evident that Eq. (23) is exponentially stable for any initial state $\tilde{\boldsymbol{x}}(0) \in \mathbb{M}_2$ and $|\phi_{\mathrm{ri}}(0)| \le 2\pi$, whenever $K > 0$. Thus, from Eqs. (13) and (23), one gets

$$\lim_{t\to\infty} y_4(t) = \lim_{t\to\infty}\left[\phi_{\mathrm{ri}}(t) - \phi_{\mathrm{ri}}^d\right] = 0 \qquad \square$$

Remark 2: The ϕ_{ri} – hold controller can be viewed as an assistant part to the output-tracking controller. As shown in Sec. V, it is necessary and crucial to obtain the nonlinear dynamic inversion and design the corresponding NDI-based output-tracking controller. Another objective of the ϕ_{ri} – hold controller is to keep the state ϕ_{ri} at the desired value ϕ_{ri}^d, which might be helpful to control followers in the same plane as expected in the close-formation flight for achieving a drag reduction. In view of Eq. (21), one sees that the ϕ_{ri} – hold controller not only depends on the partial states (ϕ_{ri}, ψ_{ri}, θ_{ri}), which are feedbacks from the subsystems I and II, but also depends on the feedforward control inputs (u_3, u_4) from the subsystem I.

The function of design parameter K is to adjust the response time of ϕ_{ri}. The larger it is, the faster the response time will be. If we can select an appropriate $K > 0$ such that the relative roll angle ϕ_{ri} tends to ϕ_{ri}^d within an acceptable short time, then it is advantageous to the implementation of output-tracking controller.

Remark 3: From the statement of problem 1 and the two controllers described by Eqs. (18) and (21), we find that there are still many freedoms to design the desirable controllers when some

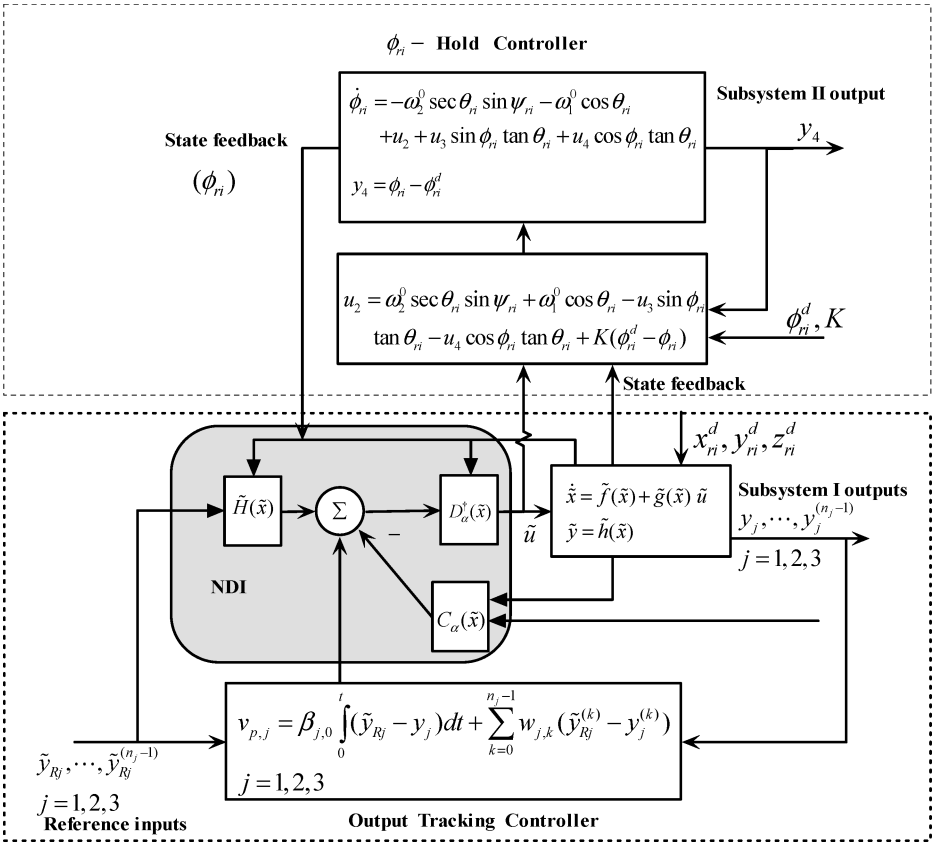

Fig. 3 Closed-loop system under the dual-controller approach.

practical factors (such as control input availability and response performance) are taken into account. These design freedoms include the design parameters in Eqs. (19) and (21) as well as the reference input signal. As pointed out in the section of problem statement, the translational and angular velocities that are controlled by an inner-loop system are used as available inputs in this study. Because these variables can have significant dynamics that is critical to the control problem and might not be changed rapidly, the reference input signal and all of the design parameters in Eqs. (19) and (21) should be chosen carefully according to the available performance of aircraft inner-loop autopilot system.

Now we are in a position to show how the two controllers work together in an interactional way. To understand the application process of the dual-controller approach as a whole, a schematic representation is depicted in Fig. 3. As illustrated in the figure, the upper part is the $\phi_{\text{ri}}-$hold controller, whereas the lower is the output-tracking controller. First, let us closely look at the output-tracking controller part. Based on the reference signal and current output as well as their corresponding derivatives, the perturbation controller $\boldsymbol{v}_p$ is computed and then incorporated into the NDI block for generating a feedforward control input to the subsystem I. Notice that the state feedbacks from both the subsystem I and II are necessary to calculate the feedforward control input. The feedforward control input is then applied to the real plant, that is, the formation flight system. Second, we would like to give a brief explanation to the $\phi_{\text{ri}}-$hold controller part. In view of Fig. 3, the control input to the subsystem II is synthesized by using the feedforward control input and partial state feedbacks from the subsystem I as well as state feedback from the subsystem II. Only partial state feedbacks, that is, relative Euler angles, are needed to formulate the control input to the subsystem II.

VII. Simulation Results

The simulation results are presented for a typical leader–follower formation flight in this section. For the following simulation example, we considered the formation consisting of one leader aircraft and two followers.

The motion state $A_0(v_0, \omega_1^0, \omega_2^0, \omega_3^0)$ of the leader is set to be (145 m/s, 0.01 rad/s, 0.01 rad/s, −0.05 rad/s). The desired relative position vectors for the follower 1 and follower 2 are given by $(-300, -200, 100)^T$ m and $(-300, 200, 50)^T$ m, respectively, which shows that the follower 1 is required to fly at the lower left-behind position of the leader, whereas the follower 2 is expected at the lower right-behind position. Moreover, the desired relative roll angles for the two followers, that is, ϕ_{r1}^d and ϕ_{r2}^d are chosen to be 0.0 rad. The initial states for the follower 1 and follower 2 are $(-330\text{ m}, -225\text{ m}, 125\text{ m}, 0.1\text{ rad}, 0.01\text{ rad}, 0.01\text{ rad})^T$ and $(-280\text{ m}, 180\text{ m}, 65\text{ m}, 0.05\text{ rad}, 0.05\text{ rad}, 0.02\text{ rad})^T$, respectively.

To demonstrate the performance of the proposed approach, the reference input $\tilde{\boldsymbol{y}}_R$ is chosen to be of the following form:

$$\tilde{\boldsymbol{y}}_R = \left(0.5a_1 e^{-t/T_1}, 0.5a_2 e^{-t/T_2}, 0.5a_3 e^{-t/T_3}\right)^T \tag{24}$$

with

$$a_1 = x_{\text{ri}}(0) - x_{\text{ri}}^d, \qquad a_2 = y_{\text{ri}}(0) - y_{\text{ri}}^d, \qquad a_3 = z_{\text{ri}}(0) - z_{\text{ri}}^d$$

In view of Eq. (24), one finds that each component of the reference signal $\tilde{\boldsymbol{y}}_R$ exponentially converges to 0 as $t \to \infty$. Hence, the followers are expected to be forced to their desired relative positions exponentially by following the reference signal $\tilde{\boldsymbol{y}}_R$. Such an exponential convergence will be advantageous to the close-formation flight and/or collision avoidance application because it would provide some reasonable and acceptable estimations on the bounds of separation errors during the transients of formation flying.

The design parameters for the output-tracking controller and the reference inputs were set to be

$$\begin{aligned} &\beta_{1,0} = 2, \quad \beta_{1,1} = 3, \quad \beta_{1,2} = 1 \\ &\beta_{2,0} = 4, \quad \beta_{2,1} = 8, \quad \beta_{2,2} = 5, \quad \beta_{2,3} = 1 \\ &\beta_{3,0} = 12, \quad \beta_{3,1} = 16, \quad \beta_{3,2} = 7, \quad \beta_{3,3} = 1 \\ &T_1 = 3.0\text{ s}, \quad T_2 = 2.5\text{ s}, \quad T_3 = 2.0\text{ s} \end{aligned} \tag{25}$$

To illustrate the effect of the design parameter K in the $\phi_{\text{ri}}-$hold controller, its value for the follower 1 and 2 was picked as 10 and 5, respectively.

Figure 4 shows the time histories of states. The control inputs are plotted in Fig. 5. The output responses are illustrated in Figs. 6 and 7. Figure 8 depicts the corresponding distances between the actual and desired positions of the two followers. The relative trajectories in three-dimensional space are also shown in Fig. 9. Although the total simulation time is 30 s, only the initial 3-s histories of some variables are depicted for plotting clearly, as shown in Figs. 4d, 5b–5d, 6d, and 7d.

From Figs. 4, 6, and 7 the good stabilizing performance of $\phi_{\text{ri}}-$hold controller can be observed. It is seen that the convergence speed of ϕ_{r1} is faster than one of ϕ_{r2} because a bigger gain parameter K was used by the follower 1. The tracking performance of the output-tracking controller can be evaluated from Figs. 6–8. Initially, the errors between the actual and desired outputs of the two followers are $(-15, -12.5, 12.5)$ m and $(10, -10, 7.5)$ m, respectively. The corresponding initial $d_1(0)$ and $d_2(0)$ are 46.3681 and 31.8746 m, respectively. Figures 6 and 7 show that the outputs $y_j (j = 1, 2, 3)$ for the two followers can pseudoexponentially converge to zero by following the reference inputs $\tilde{y}_{j,R} (j = 1, 2, 3)$, which have exponential convergence rates as stated before. From Fig. 6 it is observed that in the transient period there are no overshoots for y_1 and y_4 and only small overshoots for $y_2 = 4.307$ m and $y_3 = 2.307$ m. For the follower 2 the similar results can be found from Fig. 7, where the overshoots for $y_j (j = 1, \ldots, 4)$ in the transient period are 0 m, 2.931 m, −1.053 m, and 0 rad, respectively. An

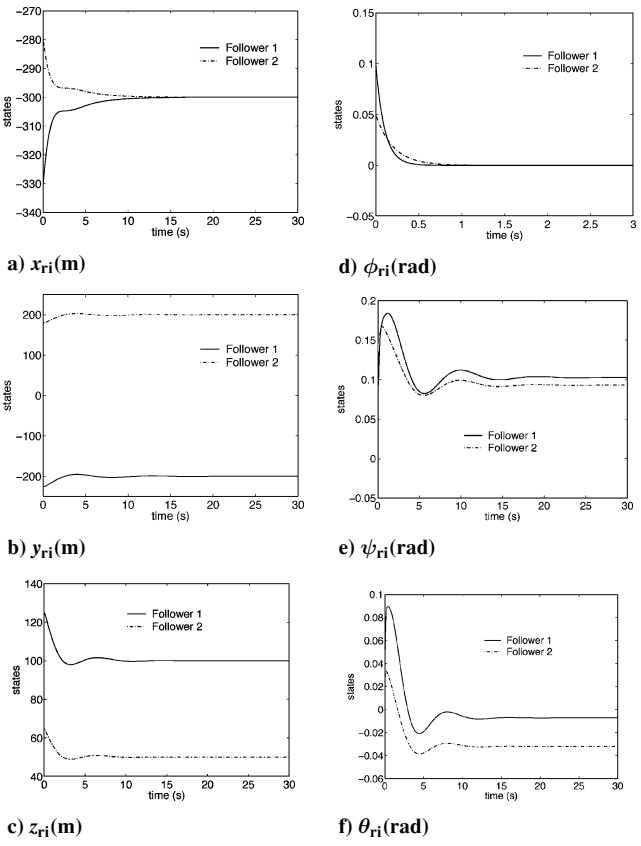

Fig. 4 Time histories of state variables.

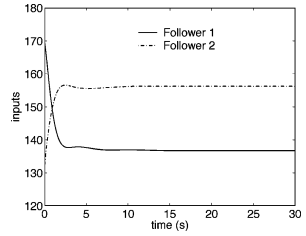

a) v_i(m/s)

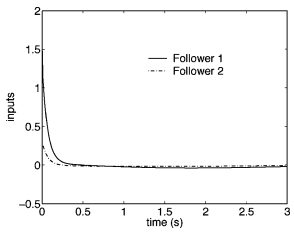

c) ω_2^i(rad/s)

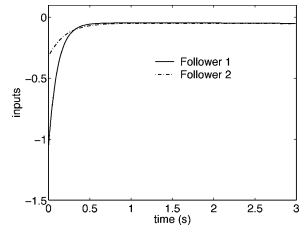

b) ω_1^i(rad/s)

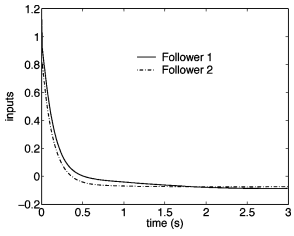

d) ω_3^i(rad/s)

Fig. 5 Control inputs.

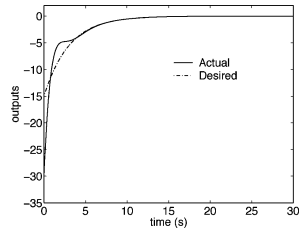

a) y_1 and y_1^d(m)

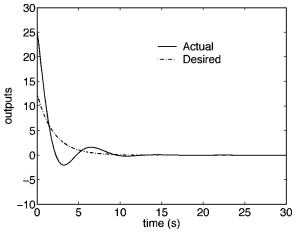

c) y_3 and y_3^d(m)

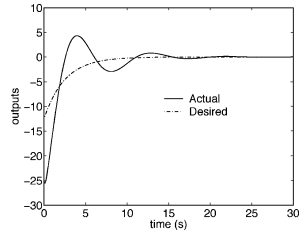

b) y_2 and y_2^d(m)

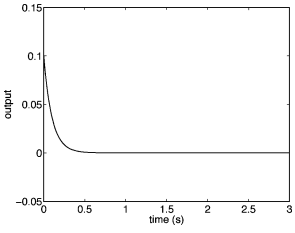

d) y_4(rad)

Fig. 6 Actual and desired outputs for the follower 1.

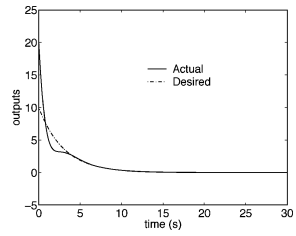

a) y_1 and y_1^d(m)

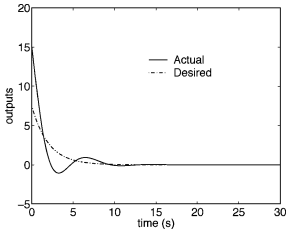

c) y_3 and y_3^d(m)

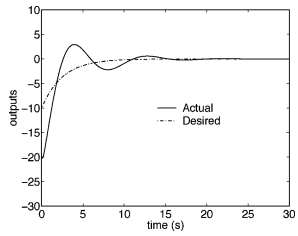

b) y_2 and y_2^d(m)

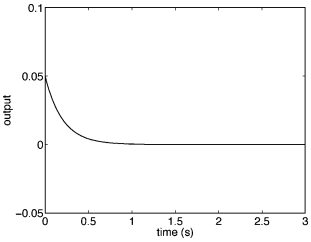

d) y_4(rad)

Fig. 7 Actual and desired outputs for the follower 2.

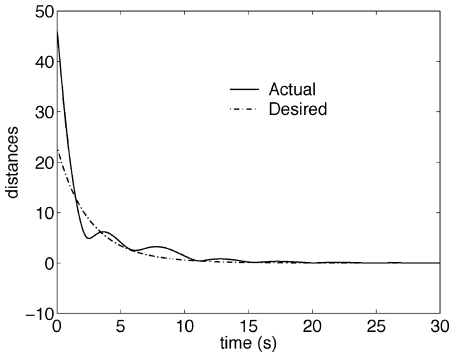

a) d_1(m)

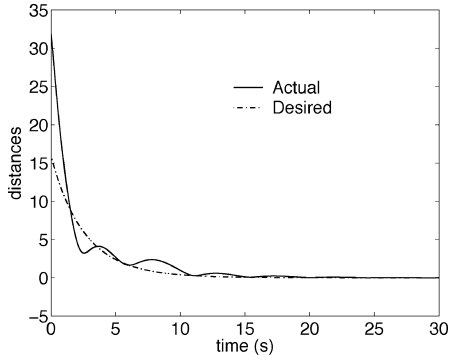

b) d_2(m)

Fig. 8 Distances between the actual and desired positions of the followers.

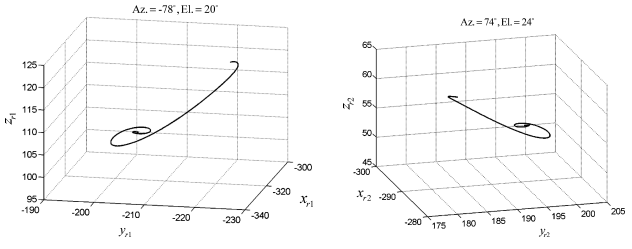

a) Follower 1 b) Follower 2

Fig. 9 Relative trajectories.

important fact that $d_j(t) < d_j(0)(j = 1, 2)$ for $t \in (0, 30]$ can be observed from Fig. 8, which is particularly interesting to the collision avoidance of formation flight.

VIII. Conclusions

Formation-keeping control is fundamental and crucial to the autonomous formation flight of multiple aircraft. This technology has many potential applications, such as close formation flight and aerial refueling. Hence, this paper dealt with the formation-keeping control problem for the three-dimensional autonomous formation flight of multiple aircraft. The full nonlinear kinematics model describing the relative position and orientation of the formation flight system has been used to develop the nonlinear formation-keeping controllers.

For the AFF system considered in this study, the main difficulties are as follows:

1) The original system has a singular decoupling matrix and does not have a well-defined vector relative degree; therefore, the traditional NDI-based output tracking methods will break down.

2) The direct use of the well-known structure algorithm, a popular method for solving the singularity problem of decoupling matrix, also fails to obtain a nonlinear dynamic inversion. To solve the aforementioned difficulties, a dual-controller approach to the three-dimensional autonomous formation control has been developed in this study. The simulation results were provided to demonstrate the excellent performance of the proposed approach.

There are several problems that remain to be explored. First, an integrated architecture for the autonomous formation flight of multiple aircraft is desirable. In such an integrated architecture, both the formation geometry control and aircraft aeronautical dynamics will be incorporated. Second, modelling and influence of vortex forces existing in the close-formation flight should be considered carefully. Further studies related to aircraft aeronautical dynamics under vortex forces resulted from a specific formation geometry are necessary. Finally, it should be one object of ongoing research to find an optimal criterion for the design parameter choice of the controllers under consideration of real-world aircraft aeronautics and formation geometry control.

Appendix A: Structure Algorithm

A brief introduction to the structure algorithm is given in the following. For the details the reader is referred to Refs. 19–22.

Given a smooth nonlinear affine control system with a singular decoupling matrix,

$$\dot{\boldsymbol{x}} = \boldsymbol{f}(\boldsymbol{x}) + \boldsymbol{g}(\boldsymbol{x})\boldsymbol{u}, \qquad \boldsymbol{y} = \boldsymbol{h}(\boldsymbol{x}) \tag{A1}$$

where $\boldsymbol{x} \in \mathbb{M} \subset \mathbb{R}^n$, $\mathbb{M}$ is a real analytic manifold, $\boldsymbol{y} = (y_1, \ldots, y_p)^T \in \mathbb{R}^p$, $\boldsymbol{u} = (u_1, \ldots, u_m)^T \in \mathbb{R}^m$. $\boldsymbol{f}(\boldsymbol{x})$, $\boldsymbol{g}(\boldsymbol{x}) = (\boldsymbol{g}_1(\boldsymbol{x}), \ldots, \boldsymbol{g}_m(\boldsymbol{x}))$ are smooth vector fields, and $\boldsymbol{h}(\boldsymbol{x}) = (h_1(\boldsymbol{x}), \ldots, h_p(\boldsymbol{x}))^T$ is a smooth vector function defined on an open set of $\mathbb{M}$.

The nonlinear inverse of system (A1) is constructed by differentiating the output y a sufficient number of times until a nonsingular decoupling matrix is obtained. Beginning with system (A1), we obtain a new system through differentiating the output y and permuting the components so that the first $r_1 := \text{Rank}[L_g \boldsymbol{h}(\boldsymbol{x})]$ are independent while zeroing the last $p - r_1$ rows with $E_1^1(\boldsymbol{x})$ and $E_1^2(\boldsymbol{x})$, respectively. Let $\mathbb{M}_1$ denote an open and dense submanifold of $\mathbb{M}$:

System 1:

$$\dot{\boldsymbol{x}} = \boldsymbol{f}(\boldsymbol{x}) + \boldsymbol{g}(\boldsymbol{x})\boldsymbol{u}, \qquad \boldsymbol{x} \in \mathbb{M}_1$$

$$z_1 = \boldsymbol{c}_1(\boldsymbol{x}) + \boldsymbol{D}_1(\boldsymbol{x})\boldsymbol{u} \tag{A2}$$

where

$$z_1 = \boldsymbol{E}_1^2(\boldsymbol{x})\boldsymbol{E}_1^1(\boldsymbol{x})\dot{\boldsymbol{y}}$$

$$= \boldsymbol{E}_1^2(\boldsymbol{x})\boldsymbol{E}_1^1(\boldsymbol{x})[L_f \boldsymbol{h}(\boldsymbol{x}) + L_g \boldsymbol{h}(\boldsymbol{x})\boldsymbol{u}]$$

$$\boldsymbol{c}_1(\boldsymbol{x}) = [\bar{\boldsymbol{c}}_1(\boldsymbol{x}), \hat{\boldsymbol{c}}_1(\boldsymbol{x})]^T, \qquad \boldsymbol{D}_1(\boldsymbol{x}) = [\bar{\boldsymbol{D}}_1(\boldsymbol{x}), \boldsymbol{0}]^T$$

$$r_1 = \text{Rank}[\bar{\boldsymbol{D}}_1(\boldsymbol{x})]$$

$$z_1 = (\bar{z}_1, \hat{z}_1)^T, \qquad \bar{z}_1 \in \mathbb{R}^{r_1}, \qquad \hat{z}_1 \in \mathbb{R}^{p-r_1}$$

$$\bar{z}_1 = \bar{\boldsymbol{c}}_1(\boldsymbol{x}) + \bar{\boldsymbol{D}}_1(\boldsymbol{x})\boldsymbol{u}, \qquad \hat{z}_1 = \hat{\boldsymbol{c}}_1(\boldsymbol{x})$$

System 2: Let $\boldsymbol{y}^{(1)} \in \mathbb{Y}_1 = \mathbb{R}^p$ and set $\mathbb{M}_2 \times \mathbb{Y}_1^1 = \{(\boldsymbol{x}, \boldsymbol{y}^{(1)}) \in \mathbb{M}_1 \times \mathbb{Y}_1 | \text{Rank}[\bar{\boldsymbol{D}}_1(\boldsymbol{x}, \boldsymbol{y}^{(1)})] = r_2\}$. Assume that $\mathbb{M}_2$ is an open dense submanifold of $\mathbb{M}_1$. Differentiate $\hat{z}_1$ and make the similar permuting and reordering as well as zeroing steps to obtain the system 2 as follows:

$$\dot{\boldsymbol{x}} = \boldsymbol{f}(\boldsymbol{x}) + \boldsymbol{g}(\boldsymbol{x})\boldsymbol{u}, \qquad z_2 = \boldsymbol{c}_2(\boldsymbol{x}) + \boldsymbol{D}_2(\boldsymbol{x})\boldsymbol{u} \tag{A3}$$

where

$$\mathbb{M}_2 \subset \mathbb{M}_1, \qquad \mathbb{Y}_1^1 \subset \mathbb{Y}_1$$

$$z_2 = \boldsymbol{E}_2^2(\boldsymbol{x})\boldsymbol{E}_2^1(\boldsymbol{x})\dot{z}_1$$

$$= \boldsymbol{E}_2^2(\boldsymbol{x})\boldsymbol{E}_2^1(\boldsymbol{x})(\bar{z}_1 + \dot{\hat{z}}_1)^T$$

$$\boldsymbol{c}_2(\boldsymbol{x}) = [\bar{\boldsymbol{c}}_2(\boldsymbol{x}), \hat{\boldsymbol{c}}_2(\boldsymbol{x})]^T, \qquad \boldsymbol{D}_2(\boldsymbol{x}) = [\bar{\boldsymbol{D}}_2(\boldsymbol{x}), \boldsymbol{0}]^T$$

$$r_2 = \text{Rank}[\bar{D}_2(x)]$$

$$z_2 = (\bar{z}_2, \hat{z}_2)^T, \qquad \bar{z}_2 \in \mathbb{R}^{r_2}, \qquad \hat{z}_2 \in \mathbb{R}^{p-r_2}$$

$$\bar{z}_2 = \bar{\boldsymbol{c}}_2(\boldsymbol{x}) + \bar{\boldsymbol{D}}_2(\boldsymbol{x})\boldsymbol{u}, \qquad \hat{z}_2 = \hat{\boldsymbol{c}}_2(\boldsymbol{x})$$

in which $\boldsymbol{E}_2^1(\boldsymbol{x})$ and $\boldsymbol{E}_2^2(\boldsymbol{x})$ denote the permutation matrix and row zeroing matrices, respectively.

System k: This algorithm can be continued in the similar way as used for obtaining system 2. It is straightforward to obtain the system k of the following form:

$$\dot{\boldsymbol{x}} = \boldsymbol{f}(\boldsymbol{x}) + \boldsymbol{g}(\boldsymbol{x})\boldsymbol{u}, \qquad z_k = \boldsymbol{c}_k(\boldsymbol{x}) + \boldsymbol{D}_k(\boldsymbol{x})\boldsymbol{u} \tag{A4}$$

where

$$\left[\boldsymbol{x}, \boldsymbol{y}^{(1)}, \ldots, \boldsymbol{y}^{(k-1)}\right] \in \mathbb{M}_k \times \mathbb{Y}_1^{k-1} \times \mathbb{Y}_2^{k-2} \cdots \times \mathbb{Y}_{k-1}^1$$

$$z_k = \boldsymbol{E}_k^2(\boldsymbol{x})\boldsymbol{E}_v^1(\boldsymbol{x})\dot{z}_{k-1}$$

$$= \boldsymbol{E}_k^2(\boldsymbol{x})\boldsymbol{E}_k^1(\boldsymbol{x})(\bar{z}_{k-1} + \dot{\hat{z}}_{k-1})^T$$

$$\boldsymbol{c}_k(\boldsymbol{x}) = [\bar{\boldsymbol{c}}_k(\boldsymbol{x}), \hat{\boldsymbol{c}}_k(\boldsymbol{x})]^T, \qquad \boldsymbol{D}_k(\boldsymbol{x}) = [\bar{\boldsymbol{D}}_k(\boldsymbol{x}), \boldsymbol{0}]^T$$

$$r_k = \text{Rank}[\bar{\boldsymbol{D}}_k(\boldsymbol{x})]$$

$$z_k = (\bar{z}_k, \hat{z}_k)^T, \qquad \bar{z}_k \in \mathbb{R}^{r_k}, \qquad \hat{z}_k \in \mathbb{R}^{p-r_k}$$

$$\bar{z}_k = \bar{\boldsymbol{c}}_k(\boldsymbol{x}) + \bar{\boldsymbol{D}}_k(\boldsymbol{x})\boldsymbol{u}, \qquad \hat{z}_k = \hat{\boldsymbol{c}}_k(\boldsymbol{x})$$

where $\boldsymbol{E}_k^1(\boldsymbol{x})$ and $\boldsymbol{E}_k^2(\boldsymbol{x})$ denote the permutation matrix and row zeroing matrices, respectively. The structure algorithm produces a sequence of nonnegative integers r_i that satisfy $0 \le r_1 \le r_2 \le \cdots \le m$. The relative order α of system (A1) is the least positive integer k^* such that $r_{k^*} \le \min(m, p)$ or $\alpha = \infty$ if the procedure runs for infinite steps. The relative order α indicates the highest-order derivative required to derive the inverse.

Appendix B: Symbols

$$c_{21} = \omega_3^0 v_0 + \omega_1^0 \omega_2^0 x_{\text{ri}} - \left(\omega_1^0\right)^2 y_{\text{ri}} - \left(\omega_3^0\right)^2 y_{\text{ri}} + \omega_2^0 \omega_3^0 z_{\text{ri}}$$

$$+ \omega_3^0 D_1^* \sec^2 \psi_{\text{ri}} + \left[\left(\omega_2^0\right)^2 x_{\text{ri}} + \left(\omega_3^0\right)^2 x_{\text{ri}} - \omega_1^0 \omega_2^0 y_{\text{ri}} - \omega_1^0 \omega_3^0 z_{\text{ri}}\right]$$

$$\times \tan \psi_{\text{ri}} - D_1^* \sec^2 \psi_{\text{ri}} \left(\omega_1^0 \cos \psi_{\text{ri}} + \omega_2^0 \sin \psi_{\text{ri}}\right) \tan \theta_{\text{ri}}$$

$$c_{31} = -\tfrac{1}{8} \sec^2 \psi_{\text{ri}} \sec^2 \theta_{\text{ri}} \Big\{ -4\omega_2^0 v_0 - 2\omega_1^0 \omega_3^0 x_{\text{ri}} + 4\omega_2^0 \omega_3^0 y_{\text{ri}}$$

$$+ 2\left(\omega_1^0\right)^2 z_{\text{ri}} - 4\left(\omega_2^0\right)^2 z_{\text{ri}} + 2\omega_1^0 \left(-\omega_3^0 x_{\text{ri}} + \omega_1^0 z_{\text{ri}}\right) \cos(2\psi_{\text{ri}})$$

$$+ 2\,\omega_3^0 D_1^* \cos(\psi_{\text{ri}} - 2\theta_{\text{ri}}) - \omega_1^0 \omega_3^0 x_{\text{ri}} \cos[2(\psi_{\text{ri}} - \theta_{\text{ri}})]$$

$$+ \left(\omega_1^0\right)^2 z_{\text{ri}} \cos[2(\psi_{\text{ri}} - \theta_{\text{ri}})] + 4\omega_2^0 v_0 \cos(2\theta_{\text{ri}})$$

$$- 2\omega_1^0 \omega_3^0 x_{\text{ri}} \cos(2\theta_{\text{ri}}) - 4\omega_2^0 \omega_3^0 y_{\text{ri}} \cos(2\theta_{\text{ri}})$$

$$+ 2\left(\omega_1^0\right)^2 z_{\text{ri}} \cos(2\theta_{\text{ri}}) + 4\left(\omega_2^0\right)^2 z_{\text{ri}} \cos(2\theta_{\text{ri}})$$

$$- \omega_1^0 \omega_3^0 x_{\text{ri}} \cos[2(\psi_{\text{ri}} + \theta_{\text{ri}})] + \left(\omega_1^0\right)^2 z_{\text{ri}} \cos[2(\psi_{\text{ri}} + \theta_{\text{ri}})]$$

$$+ 2\omega_3^0 v_0 \cos(\psi_{\text{ri}} + 2\theta_{\text{ri}}) - 2\left(\omega_3^0\right)^2 y_{\text{ri}} \cos(\psi_{\text{ri}} + 2\theta_{\text{ri}})$$

$$+ 2\omega_2^0 \omega_3^0 z_{\text{ri}} \cos(\psi_{\text{ri}} + 2\theta_{\text{ri}}) + 2\omega_1^0 v_0 \sin(2\psi_{\text{ri}})$$

$$- 2\omega_1^0 \omega_3^0 y_{\text{ri}} \sin(2\psi_{\text{ri}}) + 2\omega_1^0 \omega_2^0 z_{\text{ri}} \sin(2\psi_{\text{ri}})$$

$$- 2\left(\omega_2^0\right)^2 x_{\text{ri}} \sin(\psi_{\text{ri}} - 2\theta_{\text{ri}}) - 2\left(\omega_3^0\right)^2 x_{\text{ri}} \sin(\psi_{\text{ri}} - 2\theta_{\text{ri}})$$

$$+ 2\omega_1^0 \omega_2^0 y_{\text{ri}} \sin(\psi_{\text{ri}} - 2\theta_{\text{ri}}) + 2\omega_1^0 \omega_3^0 z_{\text{ri}} \sin(\psi_{\text{ri}} - 2\theta_{\text{ri}})$$

$$+ \omega_1^0 v_0 \sin[2(\psi_{\text{ri}} - \theta_{\text{ri}})] - \omega_1^0 \omega_3^0 y_{\text{ri}} \sin[2(\psi_{\text{ri}} - \theta_{\text{ri}})]$$

$$+ \omega_1^0 \omega_2^0 z_{\text{ri}} \sin[2(\psi_{\text{ri}} - \theta_{\text{ri}})] + \omega_1^0 v_0 \sin[2(\psi_{\text{ri}} + \theta_{\text{ri}})]$$

$$- \omega_1^0\omega_3^0 y_{\mathrm{ri}} \sin[2(\psi_{\mathrm{ri}} + \theta_{\mathrm{ri}})] + \omega_1^0\omega_2^0 z_{\mathrm{ri}} \sin[2(\psi_{\mathrm{ri}} + \theta_{\mathrm{ri}})]$$

$$+ 2\left(\omega_2^0\right)^2 x_{\mathrm{ri}} \sin(\psi_{\mathrm{ri}} + 2\theta_{\mathrm{ri}}) + 2\left(\omega_3^0\right)^2 x_{\mathrm{ri}} \sin(\psi_{\mathrm{ri}} + 2\theta_{\mathrm{ri}})$$

$$- 2\omega_1^0\omega_2^0 y_{\mathrm{ri}} \sin(\psi_{\mathrm{ri}} + 2\theta_{\mathrm{ri}}) - 2\omega_1^0\omega_3^0 z_{\mathrm{ri}} \sin(\psi_{\mathrm{ri}} + 2\theta_{\mathrm{ri}})\Big\}$$

$$D_1^* = -v_0 + \omega_3^0 y_{\mathrm{ri}} - \omega_2^0 z_{\mathrm{ri}}$$

$$D_2^* = v_0 - \omega_3^0 y_{\mathrm{ri}} + \omega_2^0 z_{\mathrm{ri}} + \dot{y}_1$$

$$d_{21} = \tfrac{1}{2}\Big\{-\omega_3^0 \cos\psi_{\mathrm{ri}} \cos\theta_{\mathrm{ri}} + \tfrac{1}{2}\omega_3^0[-3 + \cos(2\psi_{\mathrm{ri}})]$$

$$\times \cos(\theta_{\mathrm{ri}}) \sec(\psi_{\mathrm{ri}}) - 2\sin\theta_{\mathrm{ri}}\left(\omega_1^0 + \omega_2^0 \tan\psi_{\mathrm{ri}}\right)\Big\}$$

$$d_{22} = \sec^2\psi_{\mathrm{ri}} \sec\theta_{\mathrm{ri}} \sin\phi_{\mathrm{ri}} D_2^*$$

$$d_{23} = \sec^2\psi_{\mathrm{ri}} \sec\theta_{\mathrm{ri}} \cos\phi_{\mathrm{ri}} D_2^*$$

$$d_{31} = \tfrac{1}{2}\Big\{2\omega_2^0 \cos\psi_{\mathrm{ri}} \cos\theta_{\mathrm{ri}} + \omega_2^0 \sec\psi_{\mathrm{ri}} \sec\theta_{\mathrm{ri}} - \cos\theta_{\mathrm{ri}} \sec\psi_{\mathrm{ri}}\Big[\omega_2^0$$

$$+ \omega_1^0 \sin(2\psi_{\mathrm{ri}})\Big] + 2\omega_3^0 \sin\theta_{\mathrm{ri}} \tan\psi_{\mathrm{ri}} + \omega_2^0 \sec\psi_{\mathrm{ri}} \sin\theta_{\mathrm{ri}} \tan\theta_{\mathrm{ri}}\Big\}$$

$$d_{32} = -\sec\psi_{\mathrm{ri}} \sec\theta_{\mathrm{ri}}(\cos\phi_{\mathrm{ri}} \sec\theta_{\mathrm{ri}} + \sin\phi_{\mathrm{ri}} \tan\psi_{\mathrm{ri}} \tan\theta_{\mathrm{ri}}) D_2^*$$

$$d_{33} = \sec^2\psi_{\mathrm{ri}} \sec^2\theta_{\mathrm{ri}}(\cos\psi_{\mathrm{ri}} \sin\phi_{\mathrm{ri}} - \cos\phi_{\mathrm{ri}} \sin\psi_{\mathrm{ri}} \sin\theta_{\mathrm{ri}}) D_2^*$$

$$d_{21}^{\alpha} = \Big\{\cos\phi_{\mathrm{ri}}\left(\omega_2^0 \cos\psi_{\mathrm{ri}} - \omega_1^0 \sin\psi_{\mathrm{ri}}\right)$$

$$+ \sin\phi_{\mathrm{ri}}\Big[\omega_3^0 \cos\theta_{\mathrm{ri}} + \left(\omega_1^0 \cos\psi_{\mathrm{ri}} + \omega_2^0 \sin\psi_{\mathrm{ri}}\right)\sin\theta_{\mathrm{ri}}\Big]\Big\}\Big/ D_2^*$$

$$d_{22}^{\alpha} = [\cos\psi_{\mathrm{ri}} \cos\theta_{\mathrm{ri}}(\cos\psi_{\mathrm{ri}} \sin\phi_{\mathrm{ri}} - \cos\phi_{\mathrm{ri}} \sin\psi_{\mathrm{ri}} \sin\theta_{\mathrm{ri}})]\Big/ D_2^*$$

$$d_{23}^{\alpha} = -\cos\phi_{\mathrm{ri}} \cos\psi_{\mathrm{ri}} \cos^2\theta_{\mathrm{ri}}\Big/ D_2^*$$

$$d_{31}^{\alpha} = \Big\{\sin\phi_{\mathrm{ri}}\left(-\omega_2^0 \cos\psi_{\mathrm{ri}} + \omega_1^0 \sin\psi_{\mathrm{ri}}\right)$$

$$+ \cos\phi_{\mathrm{ri}}\Big[\omega_3^0 \cos\theta_{\mathrm{ri}} + \left(\omega_1^0 \cos\psi_{\mathrm{ri}} + \omega_2^0 \sin\psi_{\mathrm{ri}}\right)\sin\theta_{\mathrm{ri}}\Big]\Big\}\Big/ D_2^*$$

$$d_{32}^{\alpha} = \cos\psi_{\mathrm{ri}} \cos\theta_{\mathrm{ri}}(\cos\phi_{\mathrm{ri}} \cos\psi_{\mathrm{ri}} + \sin\phi_{\mathrm{ri}} \sin\psi_{\mathrm{ri}} \sin\theta_{\mathrm{ri}})\Big/ D_2^*$$

$$d_{33}^{\alpha} = \cos\psi_{\mathrm{ri}} \cos^2\theta_{\mathrm{ri}} \sin\phi_{\mathrm{ri}}\Big/ D_2^*$$

$$H_{21} = \sec\psi_{\mathrm{ri}}\Big[\omega_3^0 \sec\psi_{\mathrm{ri}} + \left(\omega_1^0 + \omega_2^0 \tan\psi_{\mathrm{ri}}\right)\tan\theta_{\mathrm{ri}}\Big]$$

$$H_{31} = -\tfrac{1}{8}\sec^2\psi_{\mathrm{ri}} \sec^2\theta_{\mathrm{ri}}\Big\{6\omega_2^0 + 2\omega_2^0 \cos(2\psi_{\mathrm{ri}})$$

$$+ 2\omega_3^0 \cos(\psi_{\mathrm{ri}} - 2\theta_{\mathrm{ri}}) + \omega_2^0 \cos[2(\psi_{\mathrm{ri}} - \theta_{\mathrm{ri}})] - 2\omega_2^0 \cos(2\theta_{\mathrm{ri}})$$

$$+ \omega_2^0 \cos[2(\psi_{\mathrm{ri}} + \theta_{\mathrm{ri}})] - 2\omega_3^0 \cos(\psi_{\mathrm{ri}} + 2\theta_{\mathrm{ri}}) - 2\omega_1^0 \sin(2\psi_{\mathrm{ri}})$$

$$- \omega_1^0 \sin[2(\psi_{\mathrm{ri}} - \theta_{\mathrm{ri}})] - \omega_1^0 \sin[2(\psi_{\mathrm{ri}} + \theta_{\mathrm{ri}})]\Big\}$$

Acknowledgments

The authors thank the Japan Society for the Promotion of Science and Mitsubishi Heavy Industries, Ltd., for their support. The authors are also deeply indebted to Shidong Li of San Francisco State University for his detailed suggestions and comments that considerably improved this paper. The Associate Editor and reviewers are greatly appreciated for their valuable and constructive criticism.

References

[1]Pachter, M., D'Azzo, J. J., and Dargan, J. L., "Automatic Formation Flight Control," *Journal of Guidance, Control, and Dynamics*, Vol. 17, No. 6, 1994, pp. 1380–1383.

[2]Giulietti, F., Pollini, L., and Innocenti, M., "Autonomous Formation Flight," *IEEE Control Systems Magazine*, Vol. 20, No. 6, 2000, pp. 34–44.

[3]Blake, W., and Multhopp, D., "Design, Performance and Modeling Considerations for Close Formation Flight," AIAA Paper 98-4343, Aug. 1998.

[4]Pachter, M., D'Azzo, J. J., and Proud, A. W., "Tight Formation Flight Control," *Journal of Guidance, Control, and Dynamics*, Vol. 24, No. 2, 2001, pp. 246–254.

[5]Innocenti, M., Mancino, G., Garofoli, M., and Napolitano, M., "Preliminary Analysis of Formation Flight Management," *Proceedings of AIAA Guidance, Navigation and Control Conference*, AIAA, Reston, VA, 1999, pp. 258–268; also AIAA Paper 99-3984.

[6]Hall, J. K., and Pachter, M., "Formation Maneuvers in Three Dimensions," AIAA Paper 2000-4372, Aug. 2000.

[7]Balch, T., and Arkin, R. C., "Behavior-Based Formation Control for Multirobot Teams," *IEEE Transactions on Robotics and Automation*, Vol. 14, No. 6, 1998, pp. 926–939.

[8]Schumacher, C., and Singh, S. N., "Nonlinear Control of Multiple UAVs in Close-Coupled Formation Flight," AIAA Paper 2000-4373, Aug. 2000.

[9]Singh, S. N., Zhang, R., Chandler, P., and Banda, S., "Decentralized Adaptive Close Formation Control of UAV's," AIAA Paper 2001-0106, Jan. 2001.

[10]Singh, S. N., Pachter, M., Chandler, P., Banda, S., Rasmussen, S., and Schumacher, C., "Input–Output Invertibility and Sliding Mode Control for Close Formation Flying of Multiple UAVs," *International Journal of Robust and Nonlinear Control*, Vol. 10, No. 10, 2000, pp. 779–797.

[11]Lane, S. H., and Stengel, R. F., "Flight Control Design Using Nonlinear Inverse Dynamics," *Automatica*, Vol. 24, No. 4, 1988, pp. 471–483.

[12]Ghosh, R., and Tomlin, C., "Nonlinear Inverse Dynamic Control for Mode-Based Flight," AIAA Paper 2000-4066, Aug. 2000.

[13]Devasia, S., Chen, D., and Paden, B., "Nonlinear Inversion-Based Output Tracking," *IEEE Transactions on Automatic Control*, Vol. AC-41, No. 7, 1996, pp. 930–942.

[14]Pappas, G. J., Tomlin, C., and Sastry, S., "Confict Resolution for Multi-Agent Hybrid Systems," *Proceedings of the 35th IEEE Conference on Decision and Control*, Vol. 2, IEEE Press, New York, 1996, pp. 1184–1189.

[15]Tomlin, C., Pappas, G. J., and Sastry, S., "Noncooperative Conflict Resolution," *Proceedings of the 36th IEEE Conference on Decision and Control*, Vol. 2, IEEE Press, New York, 1997, pp. 1816–1821.

[16]Tomlin, C., Pappas, G. J., and Sastry, S., "Conflict Resolution for Air Traffic Management: A Study in Multi-Agent Hybrid Systems," *IEEE Transactions on Automatic Control*, Vol. 43, No. 4, 1998, pp. 509–521.

[17]Isidori, A., *Nonlinear Control Systems*, 3rd ed., Springer-Verlag, London, 1995, pp. 219–241.

[18]Yang, E., Masuko, Y., and Mita, T., "Formation-Keeping Control with Dynamic Extension and Exact Linearization for Autonomous Formation Flight," *Proceedings of the 19th Symposium on Guidance Control*, The Society of Instrument and Control Engineers, Toyko, Japan, 2002, pp. 199–206.

[19]Kwatny, H. G., and Blankenship, G. L., *Nonlinear Control and Analytical Mechanics—A Computational Approach*, Birkhäuser, Boston, 2000, pp. 192–218.

[20]Hirschorn, R. M., "Invertibility of Multivarible Nonlinear Control Systems," *IEEE Transactions on Automatic Control*, Vol. AC-24, No. 6, 1979, pp. 855–865.

[21]Singh, S. N., "Decoupling of Invertible Nonlinear Systems with State Feedback and Precompensation," *IEEE Transactions on Automatic Control*, Vol. AC-25, No. 6, 1980, pp. 1237–1239.

[22]Singh, S. N., "A Modified Algorithm for Invertibility in Nonlinear Systems," *IEEE Transactions on Automatic Control*, Vol. AC-26, No. 2, 1981, pp. 595–598.